the spatial resolution of intrinsic signals at 569 nm was as high as 0.58 mm.

Measurement of Blood Volume Changes Based on Dye-specific Absorption Changes

Since intrinsic signals at 569 nm are considered to be proportional to Hbt concentration, the above analysis indicates that the blood volume component, as well as the Hbr component, has sufficient spatial precision to visualize individual iso-orientation domains in areas 17 and 18 of the cat visual cortex.

To further confirm our interpretation, we injected an absorption dye into the bloodstream and measured changes in blood volume on the basis of dye-specific absorption changes. Three observations provided evidence that the dye-specific absorption changes reflected changes in blood volume. First, the injections of the dye into the bloodstream caused a 17 ± 3% (mean ± SD, $n = 5$ cats) increase in light absorption. Second, the dye injections also increased the amplitude of the stimulus-nonspecific component of changes in absorption (Fig. 5*A*). The ratio of peak amplitudes before and after injections was 2.1 ± 1.1 (mean ± SD, $n = 5$). Thirdly, we found that the time courses of the stimulus-nonspecific component for the intrinsic signal at 569 nm were the same as those for the dye-specific absorption changes (Fig. 5*B*).

To examine whether stimulus-specific changes in blood volume are confined to iso-orientation domains, we compared differential images obtained before and after the dye injection (Fig. 6). If there were no stimulus-specific changes in blood volume, there would be no change in the differential image. However, the contrast of black and white patches in the differential image was in fact enhanced by the injection (Fig. 6*A*). For example, the magnitudes of stimulus-specific modulations became larger after the dye injection (Fig. 6*B*). We obtained similar results from all five cats. To quantify the results, we calculated the spatial and temporal averages (from 1 to 7 s after stimulus onset) of the stimulus-specific component of the intrinsic signals before and after the injections, and the magnitudes of the stimulus-specific components after the injections (vertical axis) were plotted against those before the injections (horizontal axis). As shown in Figure 6*C*, the magnitudes of the stimulus-specific components increased after dye injection in all five cats. These results support the proposal that there are stimulus-specific changes in blood volume.

Contribution of Changes in Blood Volume to the Intrinsic Signals in Awake Cats

To examine the blood volume component of intrinsic signals also in awake cats, we compared the intrinsic signals at 569 nm in anesthetized and awake states from the same cat. To avoid the effect of eye movements following the grating stimulus motion on the intrinsic signal in the awake state, we recorded the signal evoked by a flickering grating stimulus instead of a moving grating stimulus both in anesthetized and awake states in this experiment. We confirmed beforehand that these two stimuli elicited nearly the same responses in temporal patterns and identical response in the spatial patterns of iso-orientation domains in anesthetized cats (data not shown).

The time courses of intrinsic signals at 569 nm in the awake state were similar to those in the anesthetized state. The time to

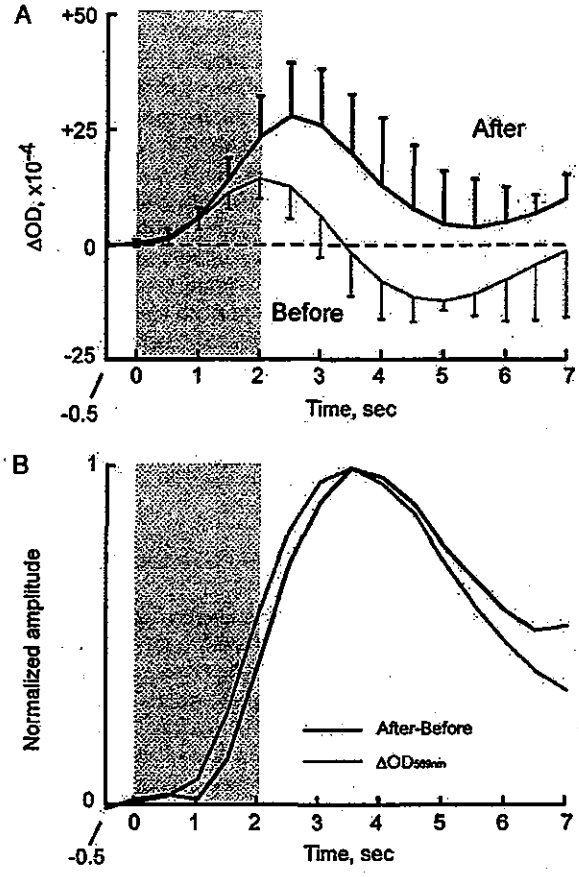

Figure 5. *Contribution* of blood volume changes to intrinsic signals. (*A*) Time courses of stimulus-nonspecific components of intrinsic signals at 620 nm before (*orange line*) and after (black line) dye injection. Error bars indicate one SD of mean obtained from five cats. (*B*) Comparison between the time course of intrinsic signals at 569 nm (green line) and that of dye-specific absorption changes (black line). Dye-specific absorption change was obtained by subtracting the absorption change at 620 nm before the injection (orange line in *A*) from that after the injection (black line in *A*). Each signal was normalized to their maximum values for comparison. The intrinsic signal at 569 nm shown here is the same data as in those shown in Figure 3*A*.

reach the peak (mean ± SD, $n = 5$ cats) of the intrinsic signal at 569 nm was 4.2 ± 0.6 s in the anesthetized state and 4.1 ± 0.46 s in the awake state. The spatial patterns of iso-orientation domains revealed by differential images at 569 nm in both states were almost identical (Fig. 7). Quantitatively, the correlation coefficient between the two images was 0.77 in this example. This value and the correlation coefficients obtained from the other four cats indicate that there is a statistically significant correlation between these images [average correlation coefficient: 0.74 ± 0.11 (mean ± SD); $P < 0.01$]. The average distance between neighboring iso-orientation domains and the average FWHM for the five awake cats was 1.26 ± 0.31 and 0.60 ± 0.10 mm respectively (mean ± SD). These values are similar to those obtained from the above-mentioned anesthetized cats. These results suggest that stimulus-specific changes in blood volume are not specific to the anesthetized state.

A difference in the intrinsic signal between the anesthetized and awake states was the magnitude of the stimulus-nonspecific and -specific components (Fig. 8). Figure 8*A* shows the average signal magnitude when the intrinsic signal at 569 nm reached its

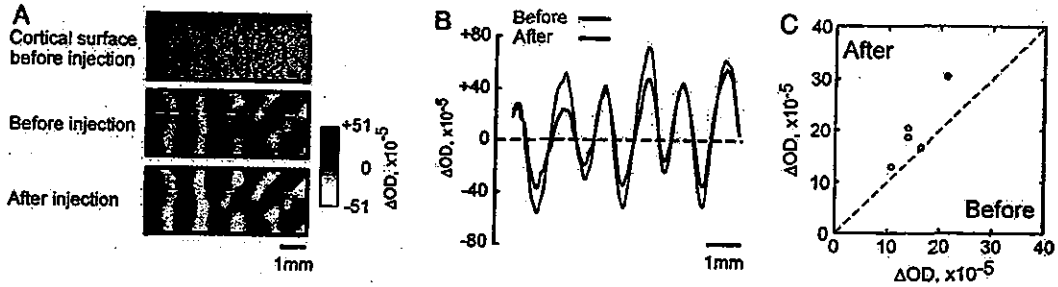

Figure 6. Stimulus-specific blood volume changes revealed by dye-specific absorption changes. (*A*) Spatial patterns of iso-orientation domains revealed by differential images before and after dye injection. The images were obtained by subtracting the responses to a grating at 90° orientation from those to a grating at 0° orientation and were temporally averaged from 1 to 7 s after stimulus onset. Borders between active and less-active domains before the injection (red lines) are superimposed on each panel. (*B*) Changes in signal intensities along the broken lines in the differential images of *A*. Black and red lines are the spatial profiles of stimulus-specific components before and after the dye injection, respectively. This result and the result shown in Figures 2 and 4*A* were obtained from the same cortical ROI. (*C*) The average magnitude of stimulus-specific components before (*x*-axis) and after (*y*-axis) the injection are plotted for five cats. Filled circle represents the result for the cat used in obtaining data shown in *A* and *B*.

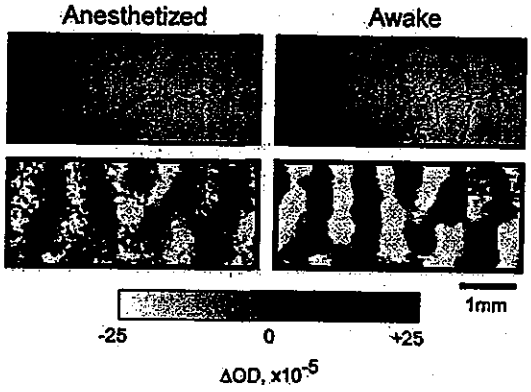

Figure 7. Maps of iso-orientation domains obtained from a cat in anesthetized and awake states. Upper panels: images of cortical surfaces taken at 538 nm from the same recording area in anesthetized and awake states. Lower panels: maps of iso-orientation domains revealed by differential images of intrinsic signals at 569 nm. The differential images were obtained by subtracting the responses evoked by an 8 Hz flickering grating at 90° orientation from the responses to a grating at 0° orientation and were temporally averaged from 1 to 7 s after stimulus onset. Borders between active and less-active domains at 569 nm in awake state (green lines) are superimposed on each panel. Recording from the anesthetized cat was conducted two days after that from the awake cats.

maximum (n = 5 cats). In the anesthetized state, neural activation induced increases in light absorption both in active and less-active domains corresponding to the stimulus-nonspecific component of the signals (Fig. 8*A*). The average magnitude of the stimulus-nonspecific component for the five cats was 15.7×10^{-3} in ΔOD. The increases in light absorption were always, though slightly, larger in the active domains of individual cats as shown by the difference in intrinsic signals between active and less-active domains (Fig. 8*B*). This difference corresponds to the stimulus-specific component of the intrinsic signal. The average magnitude of the stimulus-specific components for the five cats was 3.6×10^{-4} in ΔOD. Thus, the stimulus-specific component was only 2.3% of the stimulus-nonspecific component. The stimulus-nonspecific and stimulus-specific components of the intrinsic signal in the awake state were larger than those in the anesthetized state: the average magnitude of the stimulus-nonspecific components was 2.7 times larger and the average magnitude of stimulus-specific components was 3.6 times larger (Fig. 8*C*). The difference in magnitude ratio (2.7 versus 3.6) between stimulus-nonspecific and stimulus-specific components suggests that these two components have a different sensitivity to anesthesia.

Discussion

Spatial Localization of Changes in Blood Volume Elicited by Neural Activation

Several studies revealed the submillimeter-scale spatial localization of Hbr concentration changes in visual cortex (Malonek and Grinvald, 1996; Kim *et al*, 2000; see also Thompson *et al*, 2003). In this study, we examined the spatial precision of changes in blood volume using two different methods of analyzing reflection changes elicited by neural activation: (i) intrinsic signal imaging at the wavelength of the isosbestic point of hemoglobin, and (ii) analysis of stimulus-induced absorption changes of an intravenously infused dye. These analyses provide concrete evidence supporting a previous proposal that changes in blood volume are spatially localized (Frostig *et al*, 1990). We showed that blood volume, as well as Hbr concentration, is precisely controlled at a submillimeter-scale resolution in areas 17 and 18 of the cat visual cortex in anesthetized and awake states.

It should be pointed out that a blood volume increase includes an intravascular space increase accompanied by the dilation of vessels (increase in plasma volume) and an increase in the number of red blood cells. The measurement of the intrinsic signal at 569 nm is sensitive to the increase in the number of red blood cells. On the other hand, it is considered that the increase in dye-specific absorption change reflects the increase in plasma volume. However, we cannot exclude the possibility that the dye-specific responses also reflect the increased number of red blood cells, since we did not quantitatively examine the possibility that the dye molecules were accumulated in or bound to red blood cells. Taking into account a previous *in vivo* microscopy study (Villringer *et al*, 1994) demonstrating that increase of red blood cells in a capillary is associated with capillary dilation (i.e. increase of plasma volume) during hypercapnia, it is more plausible that these two effects — the increase in intravascular space and the increase in the number of red blood cells — are coupled and show similar behavior even when these changes are elicited by neural activation.

From the measurement of spatial separation and the size of the iso-orientation domains, we estimated the spatial resolution of blood volume changes to be as high as 0.6 mm. Recently,

Duong *et al.* (2001) have reported, using a CBF-based fMRI technique, that the size of iso-orientation domains was 0.47 mm. These results suggest that localization of blood flow changes is stronger than that of blood volume changes. In fact, unlike blood volume changes, Duong *et al.*'s experiment did not show any apparent stimulus-nonspecific component of CBF changes. They reported that the average CBF percentage-change ratio of the 'active' to 'inactive' domains was 3.3. This means that the stimulus-specific component of CBF changes was ~70% of the stimulus-nonspecific component. In contrast, this percentage was 2.3% in our measurement of blood volume changes. Further examinations are required to confirm these findings.

Limitation of Analyses of Intrinsic Signals at Multiple Wavelengths

Our analysis of intrinsic signals at multiple wavelengths is based on the assumption that intrinsic signals at visible wavelengths mainly reflect absorption changes of hemoglobin. According to this assumption, we used intrinsic signals at 569 nm as a measure of blood volume changes. We found that the time course of the intrinsic signals at 569 nm was similar to that of the dye-specific absorption changes, which supported the findings of this approach.

Although there was some supporting evidence for intrinsic signals at the isosbestic point of hemoglobin as a measure of blood volume, the isolation of components in intrinsic signals by the recording wavelengths may not be exclusive. For example, components other than hemoglobin absorption changes, such as Ls changes (MacVicar and Hochman, 1991; Kreisman *et al.*, 1995; Holthoff and Witte, 1996; Momose-Sato, 1998; Andrew *et al.*, 1999; Maheswari *et al.*, 2003; Sato *et al.*, 1997; see also Tomita *et al.*, 1983), may be involved in intrinsic signals. One way to better isolate individual components is to use a model that describes light reflection from the cortical surface (Malonek and Grinvald, 1996; Mayhew *et al.*, 1998; Nemoto *et al.*, 1999; Lindauer *et al.*, 2001). We have also analyzed our result using such a model and obtained results consistent with results described above (see Appendix). However, such analyses are not accurate and only provide semi-quantitative results because there is no exact model for changes in reflection from cortical surfaces.

Underlying Mechanisms of Stimulus-specific and Stimulus-nonspecific Components of the Blood Volume Component

In the present study, we have demonstrated that in the cat visual cortex the blood volume changes were resolved in individual iso-orientation domains ~0.6 mm in size. Taking into account the fact that the spatial separation of arteries is larger than that of functional domains, this finding suggests that fine mechanisms of blood volume control exist in fine vessel components, such as precapillary arterioles and capillaries whose spatial separations are definitely <0.6 mm (Pawlik *et al.*, 1981). The presence of such blood volume components is supported by anatomical studies showing contractile structures that may control blood flow and/or volume at the branching points of capillaries (Nakai *et al.*, 1981; Kuschinsky and Paulson, 1992; Shepro and Morel, 1993; Harrison *et al.*, 2002). This stimulus-specific component of blood volume changes, however, is only a small fraction of their stimulus-nonspecific component. To extract stimulus-specific changes in blood volume, for example, subtracting responses evoked by one orientation from those evoked by the orthogonal orientation is necessary in the visual cortex (see also for rodent barrel cortex, Hess *et al.*, 2000). There are three possibilities that explain the origins of stimulus-nonspecific components of the blood volume changes.

First, light scattering can limit the spatial resolution of optical measurement. Orbach and Cohen (1983) demonstrated that the light from a small 40 μm diameter spot spread to ~200 μm in diameter 500 μm away from the spot in cortical tissue. Because of this light scattering, stimulus-specific absorption changes can also spread into cortical domains related to the orthogonal stimulus. Thus, the stimulus-nonspecific component of the signals may be explained by the spread of the stimulus-specific component. If this is the case, however, it is difficult to explain the different ratios of signal magnitudes in the awake state to those in the anesthetized state between stimulus-specific and stimulus-nonspecific components (2.7 versus 3.6 in Fig. 8*C*).

Second, the distinction between stimulus-specific and stimulus-nonspecific components may be related to the specificity of neural activities coupled to the intrinsic signals. Assuming that synaptic activities are coupled to blood volume changes, blood volume changes can be elicited not only at regions where action potentials are generated but also at regions where

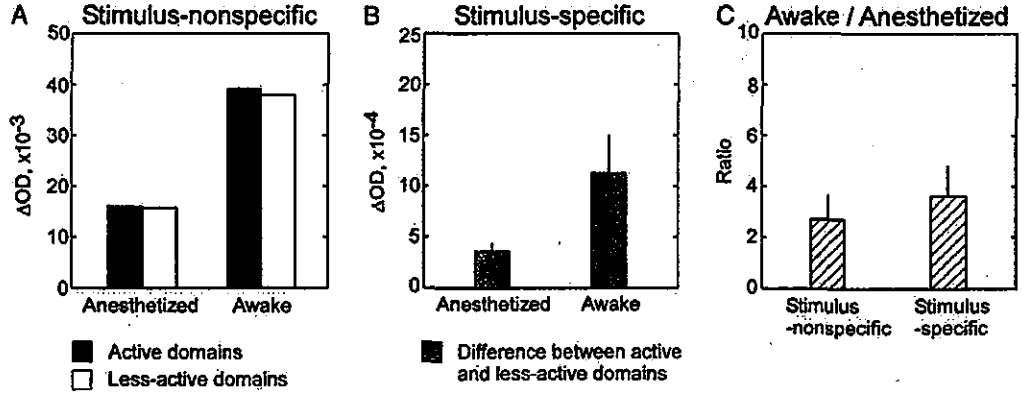

Figure 8. Comparison of signals related to blood volume changes between anesthetized and awake states. (*A*) Stimulus-nonspecific components of the intrinsic signal at 569 nm in active (solid bars) and less-active domains (open bars) for anesthetized (left column) and awake states (right column). The maximum amplitude of the signal in each cat was averaged and plotted ($n = 5$ cats). (*B*) Stimulus-specific components of the intrinsic signal at 569 nm in anesthetized (left column) and awake states (right column). (*C*) Ratios of the signal magnitude in the awake state to that in the anesthetized state for stimulus-nonspecific component (left column) and stimulus-specific component (right column). Error bars indicate one SD of mean obtained from five cats in *B* and *C*.

subthreshold synaptic potentials are generated. The stimulus-nonspecific component may reflect subthreshold synaptic potentials elicited regardless of the stimulus orientation. The mechanisms of coupling between neural activities and intrinsic signals remain issues for future investigations.

Finally, as the most plausible possibility, we consider the contribution of distinct mechanisms of blood flow control in small (precapillary, capillary) and large vessels (artery). Neural activations induce blood flow increases in arteries (Ngai *et al*, 1988, 1995; Akgoren and Lauritzen, 1999). The arteries do not necessarily govern a particular iso-orientation domain. Blood flow increases in arteries should then induce nonspecific blood volume increases in downstream small vessels (precapillary, capillary and also probably arteriole), though these vessels have a submillimeter spatial precision (but see Iadecola *et al*, 1997). Assuming supplemental blood flow control mechanisms in a capillary bed, we can expect stimulus-specific and -nonspecific components of blood volume changes. Because this proposal assumes two distinct control mechanisms, we can explain the different ratios of signal amplitudes in awake state to those in anesthetic state between stimulus-specific and stimulus-nonspecific components (*Fig. 8C*). Furthermore, the involvement of different vascular systems in the stimulus-specific and -nonspecific components of blood volume changes also explains the absence of correlation ($r = 0.43$, $P = 0.12$, $n = 14$) between the peak amplitudes of stimulus-specific and -nonspecific components.

Conclusions

In conclusion, we consider that blood volume signals in capillaries include both the stimulus-specific component controlled by the capillaries themselves and the stimulus-nonspecific component elicited by nonspecific blood inflow from upstream arteries. Because of these fine control mechanisms of blood volume, we were able to resolve submillimeter functional structures. The spatial resolution provided by these fine control mechanisms is at least 0.6 mm. This study also suggests that the visualization of blood volume changes can be used for studying brain functions at the submillimeter level.

Notes

We thank Justin Gardner for the development of a stimulus presentation program, and Kazushige Tsunoda for technical assistance throughout the experiments.

Address correspondence to Manabu Tanifuji, Laboratory for Integrative Neural Systems, RIKEN Brain Science Institute, 2-1 Hirosawa, Wakoshi, Saitama, 351-0198, Japan. Email: tanifuji@postman.riken.go.jp.

Appendix

The submillimeter-scale localization of blood volume change was also supported by an additional spectroscopic analysis as described below. We assumed that the change in optical density (ΔOD) was approximately expressed by a linear sum of changes in HbO_2 and Hbr concentrations ($\Delta[HbO_2]$ and $\Delta[Hbr]$ respectively), and Ls change (ΔLs) as follows:

$$\Delta OD(t)_\lambda = \varepsilon_\lambda^{HbO_2} \cdot d \cdot \Delta[HbO_2(t)] + \varepsilon_\lambda^{Hbr} \cdot d \cdot \Delta[Hbr(t)] - \Delta Ls(t) \qquad (2)$$

where ε_λ is the absorption coefficient at a wavelength, λ (see Fig. 1 legend for the values). The light path length, d, was assumed to be constant at these three wavelengths on the basis of our simulation study (data not shown; see also Shtoyerman *et al*, 2000). Ls change is also

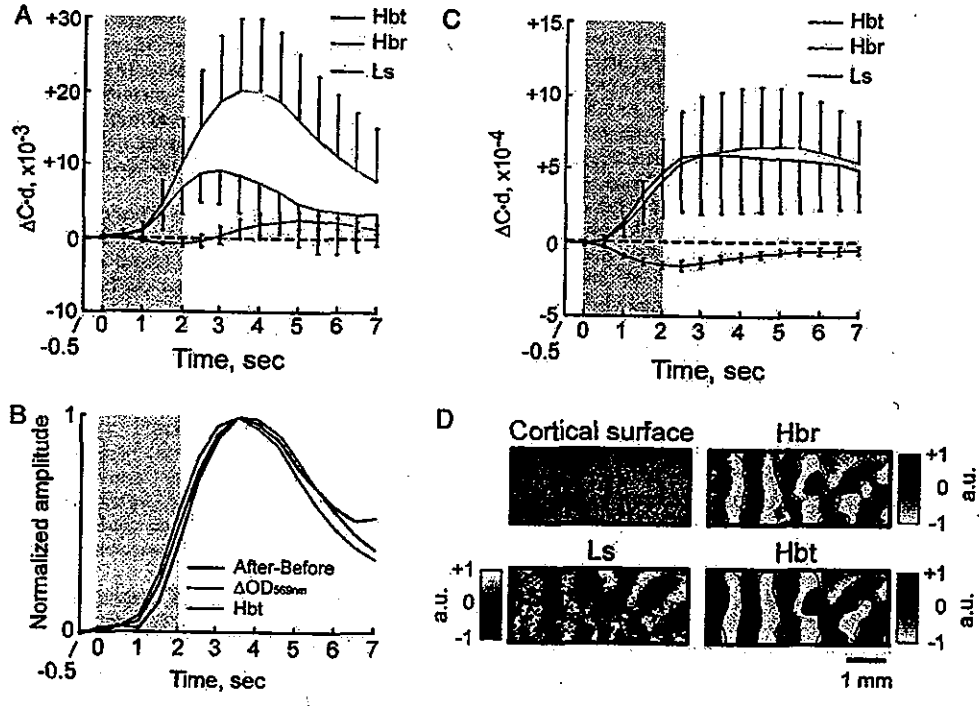

Figure 9. Results of spectroscopic analysis for intrinsic signals. (*A*) Time courses of stimulus-nonspecific components of Hbr, Hbt and Ls, which were calculated from the same data set shown in Figure 3*A*. Error bars indicate one SD of mean obtained from fourteen cats. (*B*) The time course of the Hbt (red line) was plotted together with the time courses of intrinsic signals at 569 nm (green line) and the dye-specific absorption changes (black line). Green and black lines are from the same data shown in Figure 5*B*. Each signal was normalized to its maximum values for comparison. (*C*) Time courses of stimulus-specific components of the Hbr, Hbt and Ls components. (*D*) Differential images obtained from the Hbr, Hbt and Ls. Borders between active and less-active domains at 620 nm (red lines) were superimposed on each panel. This result and the result shown in Figures 2, 4*A* and 6*A* were obtained from the same cortical ROI. Grayscales in Hbr, Hbt and Ls are arbitrary units.

assumed as a wavelength-independent variable on the basis of measurements of Ls changes in brain slices (unpublished observation; see also Cohen and Keynes, 1971; Salzberg *et al.*, 1985; Frostig *et al.*, 1990; Sato *et al.*, 1997; Momose-Sato *et al.*, 1998). The same equation was used in previous studies (Malonek and Grinvald, 1996) and yielded a good approximation for at least Hbr concentration changes in the cat visual cortex (Vanzetta and Grinvald, 1999; Thompson *et al.*, 2003).

To calculate the concentration changes of HbO_2, Hbr and the Ls component from intrinsic signals at 538, 569 and 620 nm, we analytically solved equation (2). The total hemoglobin (Hbt) concentration change was calculated as the sum of HbO_2 and Hbr concentration changes. The calculations were performed for individual stimuli and for control (blank screen) separately. Then, we subtracted the result calculated for the control (blank screen) from those for the stimuli. The product of the light path length, d, and the concentration of each component was used as a measure of each component, because d cannot be determined in the reflection measurement.

Figure 9*A* shows stimulus-induced changes in these three components. The time courses of the Ls component were biphasic, and did not vary greatly among the cats. The time courses of the Hbt concentration changes were monophasic and largely varied among the cats. To confirm whether the Hbt components faithfully represent blood volume changes, we compared the Hbt concentration changes with the stimulus-nonspecific components of the intrinsic signal at 569 nm (green line) and the dye-specific change (black line), and found these three signals showed very similar time courses (Fig. 9*B*). The time courses of the Hbr also varied among the cats. In 4 of 14 cats, the Hbr concentration initially increased after stimulus onset, reached a maximum and decreased below the baseline. However, in most cats, the changes in Hbr concentration did not cross the baseline. Consequently, the average time course of the Hbr concentrations for 14 cats was monophasic. The decrease in the Hbr concentration from the baseline in the late phase was not prominent in our study, but was in the previous studies (Malonek and Grinvald, 1996; Malonek *et al.*, 1997; Nemoto *et al.*, 1997, 1999; Mayhew *et al.*, 1999, 2000, 2001; Shtoyerman *et al.*, 2000, Jones *et al.*, 2001, Lindauer *et al.*, 2001). The discrepancy may be due to the following reasons. First, the solution based on the Beer-Lambert equation is largely affected by light pathlengths that may not be necessarily the same across the recording wavelengths used for the analysis (Mayhew *et al.*, 1999, Lindauer *et al.*, 2001). Second, time courses of intrinsic signals varied (e.g. at 607 nm, data not shown) since the relative contributions of Hbr, Hbt and Ls to the intrinsic signals may not be the same under different experimental conditions, such as individual specificity, anesthetic agents (Lindauer *et al.*, 1993), surgical procedure, recording area, stimulus type and species difference. For example, the time to reach the peak of the intrinsic signals depends on the stimulus frequency and duration (data not shown). Finally, there was no way to evaluate errors associated with the calculation of equation (2), since measurements from three wavelengths are used to obtain three parameters, the concentration changes of HbO_2, Hbr and the Ls component. Thus, in some of our measurements, we might fail to obtain reliable values of Hbr concentration changes, particularly late in the time course.

Similar to the intrinsic signals (Fig. 3*B*), the changes in Hbt and Hbr concentrations in active domains were always larger than those in less-active domains, and Ls changes in active domains were always smaller than those in less-active domains (Fig. 9*C*). To show the spatial pattern of the stimulus-specific components of Hbr, Hbt and Ls, their differential images were averaged from 1 s to 7 s after stimulus onset. As shown in Figure 9*D* the spatial pattern of the stimulus-specific component of the Hbt was almost identical to that of intrinsic signals (red contours) as well as the Hbr and Ls. The correlation coefficients between the differential images at 620 nm and that of Hbr, Hbt and Ls were 0.88, 0.87 and 0.77 ($P < 0.01$), respectively, in this example. We also calculated these correlation coefficients for the other 13 cats, and obtained statistically significant correlations for all of them ($P < 0.01$). The average correlation coefficients for 14 cats with Hbr, Hbt and Ls were 0.52 ± 0.17, 0.63 ± 0.17 and 0.79 ± 0.08, respectively. The highest correlation coefficient in the Ls is probably because of the relatively high contribution of the Ls to intrinsic signals at 620 nm.

References

Akgoren N, Lauritzen M (1999) Functional recruitment of red blood cells to rat brain microcirculation accompanying increased neuronal activity in cerebellar cortex. Neuroreport 10:3257–3263.

Andrew RD, Jarvis CR, Obeidat AS (1999) Potential sources of intrinsic optical signals imaged in live brain slices. Methods 18:185–196, 179.

Bonhoeffer T, Grinvald A (1991) Iso-orientation domains in cat visual cortex are arranged in pinwheel-like patterns. Nature 353: 429–431.

Bonhoeffer T, Grinvald A (1993) The layout of iso-orientation domains in area 18 of cat visual cortex: optical imaging reveals a pinwheel-like organization. J Neurosci 13:4157–4180.

Bonhoeffer T, Grinvald A (1996) Optical imaging based on intrinsic signals: the methodology. In: Brain mapping: the methods (Toga AW, Mazziotta JC, eds), pp. 55–97. San Diego, CA: Academic Press.

Bonhoeffer T, Kim DS, Malonek D, Shoham D, Grinvald A (1995) Optical imaging of the layout of functional domains in area 17 and across the area 17/18 border in cat visual cortex. Eur J Neurosci 7: 1973–1988.

Cannestra AF, Pouratian N, Shomer MH, Toga AW (1998) Refractory periods observed by intrinsic signal and fluorescent dye imaging. J Neurophysiol 80:1522–1532.

Cohen LB, Keynes RD (1971) Changes in light scattering associated with the action potential in crab nerves. J Physiol 212:259–275.

Duong TQ, Kim DS, Ugurbil K, Kim SG (2001) Localized cerebral blood flow response at submillimeter columnar resolution. Proc Natl Acad Sci USA 98:10904–10909.

Frostig RD, Lieke EE, Ts'o DY, Grinvald A (1990) Cortical functional architecture and local coupling between neuronal activity and the microcirculation revealed by *in vivo* high-resolution optical imaging of intrinsic signals. Proc Natl Acad Sci USA 87:6082–6086.

Ghose GM, Ts'o DY (1997) Form processing modules in primate area V4. J Neurophysiol 77:2191–2196.

Grinvald A, Lieke E, Frostig RD, Gilbert CD, Wiesel TN (1986) Functional architecture of cortex revealed by optical imaging of intrinsic signals. Nature 324:361–364.

Harrison RV, Harel N, Panesar J, Mount RJ (2002) Blood capillary distribution correlates with hemodynamic-based functional imaging in cerebral cortex. Cereb Cortex 12:225–233.

Hess A, Stiller D, Kaulisch T, Heil P, Scheich H (2000) New insights into the hemodynamic blood oxygenation level-dependent response through combination of functional magnetic resonance imaging and optical recording in gerbil barrel cortex. J Neurosci 20: 3328–3338.

Holthoff K, Witte OW (1996) Intrinsic optical signals in rat neocortical slices measured with near-infrared dark-field microscopy reveal changes in extracellular space. J Neurosci 16:2740–2749.

Iadecola C, Yang G, Ebner TJ, Chen G (1997) Local and propagated vascular responses evoked by focal synaptic activity in cerebellar cortex. J Neurophysiol 78:651–659.

Jones M, Berwick J, Johnston D, Mayhew J (2001) Concurrent optical imaging spectroscopy and laser-Doppler flowmetry: the relationship between blood flow, oxygenation, and volume in rodent barrel cortex. Neuroimage 13:1002–1015.

Kim DS, Duong TQ, Kim SG (2000) High-resolution mapping of iso-orientation columns by fMRI. Nat Neurosci 3:164–169.

Kreisman NR, LaManna JC, Liao SC, Yeh ER, Alcala JR (1995) Light transmittance as an index of cell volume in hippocampal slices: optical differences of interfaced and submerged positions. Brain Res 693:179–186.

Kuschinsky W, Paulson OB (1992) Capillary circulation in the brain. Cerebrovasc Brain Metab Rev 4:261–286.

Lindauer U, Villringer A, Dirnagl U (1993) Characterization of CBF response to somatosensory stimulation: model and influence of anesthetics. Am J Physiol 264:H1223–1228.

Lindauer U, Royl G, Leithner C, Kuhl M, Gold L, Gethmann J, Kohl-Bareis M, Villringer A, Dirnagl U (2001) No evidence for early decrease in blood oxygenation in rat whisker cortex in response to functional activation. Neuroimage 13:988–1001.

Maheswari RU, Takaoka H, Kadono H, Homma R, Tanifuji M (2003) Novel functional imaging technique from brain surface with optical

coherence tomography enabling visualization of depth resolved functional structure *in vivo*. J Neurosci Methods 124:83–92.
MacVicar BA, Hochman D (1991) Imaging of synaptically evoked intrinsic optical signals in hippocampal slices. J Neurosci 11:1458–1469.
Malonek D, Grinvald A (1996) Interactions between electrical activity and cortical microcirculation revealed by imaging spectroscopy: implications for functional brain mapping. Science 272:551–554.
Malonek D, Tootell RB, Grinvald A (1994) Optical imaging reveals the functional architecture of neurons processing shape and motion in owl monkey area MT. Proc R Soc Lond B Biol Sci 258:109–119.
Malonek D, Dirnagl U, Lindauer U, Yamada K, Kanno I, Grinvald A (1997) Vascular imprints of neuronal activity: relationships between the dynamics of cortical blood flow, oxygenation, and volume changes following sensory stimulation. Proc Natl Acad Sci USA 94:14826–14831.
Mayhew J, Hu D, Zheng Y, Askew S, Hou Y, Berwick J, Coffey PJ, Brown N (1998) An evaluation of linear model analysis techniques for processing images of microcirculation activity. Neuroimage 7:49–71.
Mayhew J, Zheng Y, Hou Y, Vuksanovic B, Berwick J, Askew S, Coffey P (1999) Spectroscopic analysis of changes in remitted illumination: the response to increased neural activity in brain. Neuroimage 10: 304–326.
Mayhew J, Johnston D, Berwick J, Jones M, Coffey P, Zheng Y (2000) Spectroscopic analysis of neural activity in brain: increased oxygen consumption following activation of barrel cortex. Neuroimage 12: 664–675.
Mayhew J, Johnston D, Martindale J, Jones M, Berwick J, Zheng Y (2001) Increased oxygen consumption following activation of brain: theoretical footnotes using spectroscopic data from barrel cortex. Neuroimage 13:975–987.
Momose-Sato Y, Sato K, Hirota A, Kamino K (1998) GABA-induced intrinsic light-scattering changes associated with voltage-sensitive dye signals in embryonic brain stem slices: coupling of depolarization and cell shrinkage. J Neurophysiol 79:2208–2217.
Nakai K, Imai H, Kamei I, Itakura T, Komari N, Kimura H, Nagai T, Maeda T (1981) Microangioarchitecture of rat parietal cortex with special reference to vascular 'sphincters'. Scanning electron microscopic and dark field microscopic study. Stroke 12:653–659.
Narayan SM, Esfahani P, Blood AJ, Sikkens L, Toga AW (1995) Functional increases in cerebral blood volume over somatosensory cortex. J Cereb Blood Flow Metab 15:754–765.
Nemoto M, Nomura Y, Tamura M, Sato C, Houkin K, Abe H (1997) Optical imaging and measuring of local hemoglobin concentration and oxygenation changes during somatosensory stimulation in rat cerebral cortex. Adv Exp Med Biol 428:521–531.
Nemoto M, Nomura Y, Sato C, Tamura M, Houkin K, Koyanagi I, Abe H (1999) Analysis of optical signals evoked by peripheral nerve stimulation in rat somatosensory cortex: dynamic changes in hemoglobin concentration and oxygenation. J Cereb Blood Flow Metab 19:246–259.
Ngai AC, Ko KR, Morii S, Winn HR (1988) Effect of sciatic nerve stimulation on pial arterioles in rats. Am J Physiol 254:H133–139.
Ngai AC, Meno JR, Winn HR (1995) Simultaneous measurements of pial arteriolar diameter and laser-Doppler flow during somatosensory stimulation. J Cereb Blood Flow Metab 15:124–127.
Orbach HS, Cohen LB (1983) Optical monitoring of activity from many areas of the *in vitro* and *in vivo* salamander olfactory bulb: a new method for studying functional organization in the vertebrate central nervous system. J Neurosci 3:2251–2262.
Pawlik G, Rackl A, Bing RJ (1981) Quantitative capillary topography and blood flow in the cerebral cortex of cats: an *in vivo* microscopic study. Brain Res 208:35–58.
Ratzlaff EH, Grinvald A (1991) A tandem-lens epifluorescence macroscope: hundred-fold brightness advantage for wide-field imaging. J Neurosci Methods 36:127–137.
Roe AW, Ts'o DY (1995) Visual topography in primate V2: multiple representation across functional stripes. J Neurosci 15:3689–3715.
Salzberg BM, Obaid AL, Gainer H (1985) Large and rapid changes in light scattering accompany secretion by nerve terminals in the mammalian neurohypophysis. J Gen Physiol 86:395–411.
Sato K, Momose-Sato Y, Arai Y, Hirota A, Kamino K (1997) Optical illustration of glutamate-induced cell swelling coupled with membrane depolarization in embryonic brain stem slices. Neuroreport 8:3559–3563.
Shepro D, Morel NM (1993) Pericyte physiology. FASEB J 7:1031–1038.
Shtoyerman E, Arieli A, Slovin H, Vanzetta I, Grinvald A (2000) Long-term optical imaging and spectroscopy reveal mechanisms underlying the intrinsic signal and stability of cortical maps in V1 of behaving monkeys. J Neurosci 20:8111–8121.
Sibson NR, Dhankhar A, Mason GF, Rothman DL, Behar KL, Shulman RG (1998) Stoichiometric coupling of brain glucose metabolism and glutamatergic neuronal activity. Proc Natl Acad Sci USA 95:316–321.
Silver IA (1978) Cellular microenvironment in relation to local blood flow. Ciba Found Symp:49–67.
Thompson JK, Peterson MR, Freeman RD (2003) Single-neuron activity and tissue oxygenation in the cerebral cortex. Science 299: 1070–1072.
Tomita M, Gotoh F, Yamamoto M, Tanahashi N, Kobari M (1983) Effects of hemolysis, hematocrit, RBC swelling, and flow rate on light scattering by blood in a 0.26 cm ID transparent tube. Biorheology 20:485–494.
Ts'o DY, Frostig RD, Lieke EE, Grinvald A (1990) Functional organization of primate visual cortex revealed by high resolution optical imaging. Science 249:417–420.
Tsunoda K, Yamane Y, Nishizaki M, Tanifuji M (2001) Complex objects are represented in macaque inferotemporal cortex by the combination of feature columns. Nat Neurosci 4:832–838.
Vanzetta I, Grinvald A (1999) Increased cortical oxidative metabolism due to sensory stimulation: implications for functional brain imaging. Science 286:1555–1558.
Villringer A, Them A, Lindauer U, Einhaupl K, Dirnagl U (1994) Capillary perfusion of the rat brain cortex. An *in vivo* confocal microscopy study. Circ Res 75:55–62.
Wang G, Tanaka K, Tanifuji M (1996) Optical imaging of functional organization in the monkey inferotemporal cortex. Science 272: 1665–1668.
Wang G, Tanifuji M, Tanaka K (1998) Functional architecture in monkey inferotemporal cortex revealed by *in vivo* optical imaging. Neurosci Res 32:33–46.

Human Molecular Genetics, 2005, Vol. 14, No. 6 1–11
doi:10.1093/hmg/ddi069
Advance Access published on xxx

The *Pax6* isoform bearing an alternative spliced exon promotes the development of the neural retinal structure

Noriyuki Azuma[1,2,*], Keiko Tadokoro[2], Astuko Asaka[2], Masao Yamada[2], Yuki Yamaguchi[3], Hiroshi Handa[3], Satsuki Matsushima[4], Takashi Watanabe[4], Shinichi Kohsaka[5], Yasuyuki Kida[6], Tomoki Shiraishi[6], Toshihiko Ogura[6], Kenji Shimamura[7] and Masato Nakafuku[7]

[1]Department of Ophthalmology, National Center for Child Health and Development, Tokyo 157-8535, Japan, [2]Department of Genetics, National Research Institute for Child Health and Development, Tokyo 154-8567, Japan, [3]Department of Biological Information, Tokyo Institute of Technology, Graduate School of Bioscience and Biotechnology, Yokohama, 226-8501, Japan, [4]Department of Clinical Pathology, Kyorin University School of Medicine, Tokyo 181-8611, Japan, [5]Department of Neurochemistry, National Institute of Neuroscience, Tokyo, 187-8502, Japan, [6]Department of Developmental Neurobiology, Institute of Development, Aging and Cancer, Sendai 980-8575, Japan and [7]Department of Neuroscience, University of Tokyo Graduate School of Medicine, Tokyo 113-0033, Japan

Received November 28, 2004; Accepted January 18, 2005

The vertebrate retina has an area where visual cells are closely packed for proper vision that is known as a fovea, an area centralis or a visual streak. The molecular mechanism that regulates the formation of these structures and visual cell gradients is unknown. The transcription factor Pax6 is a master regulator of eye development. A Pax6 isoform that contains an exon 5a-encoded 14 amino acid insertion in its paired domain, Pax6(+5a), has different DNA-binding properties compared with the Pax6(−5a) isoform. Little is known about the functional significance of Pax6(+5a). Here, we show that Pax6(+5a) is expressed especially in the retinal portion where visual cells accumulate during eye development and, when overexpressed, induces a remarkable well-differentiated retina-like structure. Pax6(+5a) proteins that bear point mutations that are found in patients with foveal hypoplasia are unable to induce these ectopic retina-like structures. We propose that Pax6(+5a) induces a developmental cascade in the prospective fovea, area centralis or visual streak region that leads to the formation of a retinal architecture bearing densely packed visual cells.

INTRODUCTION

Most vertebrates have a region of the retina where cone photoreceptors, bipolar cells and ganglion cells accumulate and specialize, which contributes to better vision (1–3). This region comes in two general forms, namely, a visual streak and an area centralis. Animals that are nocturnal or have relatively poor vision bear a visual streak, where the photoreceptors, bipolar cells and ganglion cells congregate and become specialized along a horizontal line of the eye fundus. In contrast, animals that have relatively good vision bear the area centralis, which is a circular spot in the retina. The image of an object becomes centered on this region. A specialized form of the area centralis is the fovea, which helps many reptiles and birds, and most primates achieve greater visual sensitivity. The fovea is an area in which cone photoreceptors are highly concentrated and the inner retina is thinned. Human patients lacking the fovea have a poor visual acuity of 0.1–0.3, even with lens correction (4,5). Thus, the fovea is an essential architectural feature that is required for our sharp visual acuity.

In most vertebrates that have a fovea or an area centralis, the retinal cells first accumulate, differentiate and form synaptic connections at the prospective fovea or area centralis

*To whom correspondence should be addressed at: Department of Ophthalmology, National Center for Child Health and Development, 2-10-1 Okura, Setagaya-ku, Tokyo 157-8535, Japan. Tel: +81 334160181; Fax: +81 334162222; Email: azuma-n@ncchd.go.jp

region during the very early stages of eye development, corresponding to the time when ganglion cells appear in the retina. The differentiation of the retinal cells then progresses from the centre to the periphery, which results in a gradient of visual sensitivity (2,3). The molecular mechanisms that regulate the formation of these specific retinal structures are not well elucidated, although previous studies have explored mechanism and genes involved in differentiation of the retinal area (6–8).

Recently, patients with foveal hypoplasia were found to bear mutations in the *PAX6* gene (4,5). The *Pax6* gene encodes a transcription factor and plays important roles in eye morphogenesis in both vertebrates and invertebrates (9–12). This gene has been reported to induce ectopic eye formation in *Drosophila melanogaster* (13) and *Xenopus* larvae (14), and is known as a master control gene in eye formation (9–11). Pax6 is expressed in various eye tissues. In the neural retina, Pax6 is expressed widely in multipotent progenitor cells at early stages and to a lesser extent in ganglion, horizontal and amacrine cells at late stages (15–17). The *Pax6* gene produces two isoforms by alternative splicing, namely, Pax6(−5a) and Pax6(+5a). Pax6(+5a) differs from Pax6(−5a) by the presence of an exon 5a-encoded 14 amino acid insertion in its paired-type DNA-binding domain (paired domain, or PD) (18,19). Pax6(−5a) and Pax6(+5a) show distinct DNA-binding properties (20) and their distinct consensus binding sequences have been determined. These are termed P6CON and 5aCON, respectively (21). Mutational analyses have shown that the N-terminal subdomain (NTS) and the C-terminal subdomain (CTS) of the Pax6 PD are respectively responsible for the DNA-binding abilities of Pax6(−5a) and Pax6(+5a) and their transactivation activity (20,22). Pax6(−5a) binds to a promoter element of the *ζ-crystallin* gene at a site that is highly similar to P6CON (23), while target genes of Pax6(+5a) that bear 5aCON-like sequences are yet to be identified.

Many mutations in the *PAX6* gene have been identified in human patients with foveal hypoplasia (4,5,24–27). In most classical aniridia patients, caused by haploinsufficiency of PAX6 due to its deletion or the presence of a nonsense mutation, all other eye tissues apart from the iris, including the cornea, lens, fovea and optic nerve, are also affected. In contrast, missense mutations in the *PAX6* gene cause more specific eye anomalies (4,5,25–27), probably because Pax6 has multiple functional domains and that missense mutations in this gene disturb one or only a few of these domains. Previously, we reported two PAX6 missense mutations, R128C in the CTS of the PD and V54D in exon 5a, in Japanese patients with foveal hypoplasia (4,5). An R128C mutation was again identified in an independent European patient with the same phenotype (26). These findings suggest that the CTS and exon 5a, which are two elements that are thought to be important for the function of the Pax6(+5a) isoform, may be involved in the formation of the fovea. We investigated expression pattern of Pax6(+5a) in the developing retina and effect of the isoform in retinal development by gain-of-function experiments, and here present evidence that Pax6(+5a) contributes to promote the formation of the retinal structure.

RESULTS

Pax6(+5a) is abundantly expressed in the retinal portion where visual cells accumulate

We first examined the regional expression of the Pax6 isoforms by subjecting sections of a neonatal marmoset eye (which has a fovea) to immunohistochemical staining with two different antibodies that can distinguish between the two Pax6 isoforms. One of these antibodies, which is denoted as anti-Pax6, was raised against amino acids 1–223 including those encoded by exon 5a. This antibody reacts with both Pax6(−5a) and Pax6 (+5a), as reported previously (16,17). For this study, we raised another antibody against a synthetic peptide consisting of the 14 amino acid residues that are encoded by exon 5a (anti-exon 5a). Western blotting of proteins prepared from cultured mouse embryonic carcinoma P19 cells that had been transfected with constructs expressing Pax6(−5a) or Pax6(+5a), and of marmoset tissues expressing both isoforms demonstrated the specificity of these antibodies (Fig. 1A). On the marmoset sections, anti-Pax6 visualized three layers, namely, the ganglion cell layer and the inner and outer edges of the inner nuclear layer of the retina. The foveal region was heavily stained, and both the nasal and temporal nasal sides were also stained (Fig. 1C, middle panels). This indicates the wide distribution of Pax6 proteins throughout the entire retina. In contrast, the anti-exon 5a staining pattern suggested that the Pax6(+5a) protein localizes to a restricted retinal area between the optic nerve head and the fovea (Fig. 1C b and c). This was clear when the staining in the nasal and foveal sides of the optic nerve head was compared. The staining was identified scarcely in the nasal side but obviously in the foveal side (Fig. 1C b). From these observations, we conclude that the Pax6(+5a) isoform is expressed especially in the restricted retinal portion where the densely packed visual cells reside.

Reflecting evolutionary conservation of the amino acid sequence encoded by exon 5a, the anti-exon 5a antibody reacts with chicken Pax6(+5a) as well, albeit weakly. In the chicken retina of Hamburger–Hamilton (HH) stage 45, the Pax6(+5a) protein appears to localize in a restricted retinal area of the visual streak, whereas the Pax6(−5a) protein distributes throughout the entire retina (Fig. 2A). To compare the expression levels of the two isoforms, we next performed semi-quantitative RT–PCR analysis using dissected retinal tissues of chick embryos at HH stages 12–45. The isolated RNAs were subjected to RT–PCR analysis using specific primers that flank exon 5a and can distinguish between the two isoforms *Pax6(+5a)* and *Pax6(−5a)*. At an early developmental stage (HH stage12), when the optic vesicle is formed and multipotent progenitor cells still exist in the neural retina, the two isoforms were expressed in both the central nervous system (CNS) and the eye primordium but the *Pax6(−5a)* isoform predominated (Fig. 2B). At HH stage 20, Pax6(−5a) was still the major transcript. At this stage, the formation of the eye is proceeding and lens formation is evident. During HH stages 24–30, the ganglion cells in the retina differentiate. The level of *Pax6(−5a)* expression seems to decrease transiently at HH stage 24 and increase at HH stage 30. Interestingly, the level of *Pax6(+5a)* expression gradually increased during this period

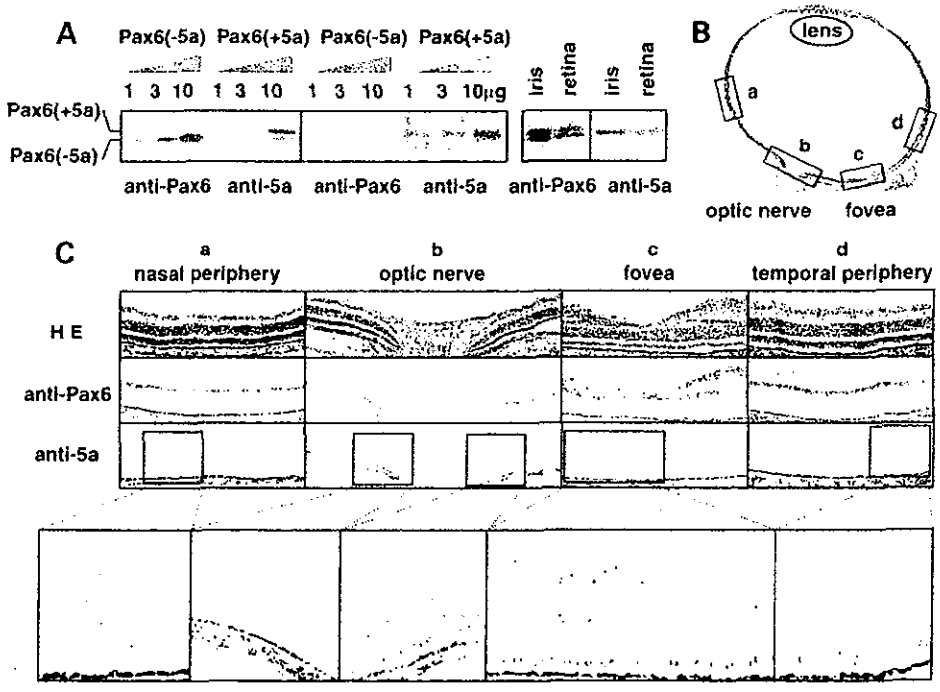

Figure 1. Histochemical analysis of the expression of the two Pax6 isoforms in the neonatal marmoset eye. (**A**) Western blotting analysis confirming the specificity of the two antibodies that were used. P19 cells (10^5 cells) were transfected with either the Pax6(−5a) or Pax6(+5a) expression construct and nuclear protein fractions obtained 24 h post-transfection were analyzed. Anti-Pax6 recognized the exogenously expressed Pax6(−5a) and Pax6(+5a) proteins as well as endogenous Pax6(−5a) protein, whereas anti-exon 5a recognized Pax6(+5a) but not Pax6(−5a). Western blotting analysis of nuclear fraction proteins obtained from the iris and retina tissues of the neonatal marmoset (*Callithrix jacchus*) also showed that anti-Pax6 recognized both native Pax6(−5a) and Pax6(+5a) proteins, whereas anti-exon 5a recognized Pax6(+5a) but not Pax6(−5a). (**B**) View of a horizontal section of the eye of a neonatal marmoset stained with HE. (**C**) Magnified fields of the eye stained with HE, anti-Pax6 or anti-exon 5a (bar scale 100 μm). Further enlarged images are shown below. a, nasal peripheral area; b, optic nerve head area; c, fovea area; d, temporal peripheral area. The staining for anti-exon 5a localizes around the fovea area, whereas that for anti-Pax6 is detected throughout the entire retina. The result shown is representative of three independent experiments using four marmoset eyes.

in all ocular tissues such as the cornea, lens and retina. Increased expression of *Pax6(+5a)* was also evident in the retina in later stages (HH stages 36–45), when all photoreceptors, horizontal and amacrine cells differentiate. Although the eyes of domestic birds lack the fovea, they possess a distinct visual streak in the posterior portion of the retina (1,2). Expression of *Pax6(+5a)* became particularly intense in this posterior portion. At HH stage 36, the expression of *Pax6(+5a)* exceeded that of *Pax6(−5a)* in the posterior retina. These observations indicate that expression of the two Pax6 isoforms are differentially regulated during retinal development, with Pax6(+5a) expression increasing only in a specified region, whereas Pax6(−5a) expression being throughout the retina.

In *ovo* misexpression of *Pax6(+5a)* gene markedly expands the retinal layer and promotes the growth and differentiation of retinal cells into visual cells

Next, we investigated the roles the two Pax6 isoforms play in the formation of the eye architecture by *in ovo* electroporation (28). Thus, an expression construct for either Pax6(+5a) or Pax6(−5a) was electroporated into the developing retina of HH stages 16–30 chick embryos, together with an expression construct of green fluorescence protein (GFP) (29) to monitor the expression of the transgenes. Expression plasmids [pCAGGS-PAX6(−5a) and pCAGGS-PAX6(+5a)] carry the entire human *PAX6* coding region with or without exon 5a under the control of a cytomegalovirus enhancer and chicken β-actin promoter, as described previously (5,22). Embryos that had been electroporated were harvested at various stages and analyzed. Retinal formation was scarcely affected when either isoform was transduced after HH stage 30 (data not shown). However, marked changes were observed when either isoform was transduced at HH stages 16–24, when the formation of the optic cup was completed. Six to twelve hours after electroporation of Pax6(−5a) and GFP (HH stage 18), the electroporated region, confirmed by staining with anti-Pax6 and anti-GFP antibodies, was found to proliferate excessively, as evidenced by intense staining with anti-5-bromo-2′-deoxyuridine (BrdU) antibody (Fig. 3). The promotion of retinal cell proliferation occurred similarly up to this stage regardless of the Pax6 isoforms overexpressed (data not shown). Electroporation of the empty vector alone, the pCAGGS-GFP or both constructs did not induce any change.

At later stages, a significant difference in the effect of the two Pax6 isoforms was observed. When Pax6(−5a) was misexpressed, 3–7 days after the electroporation (HH stages 28–35), 47% ($n = 198$) of the eyes were larger than the untreated

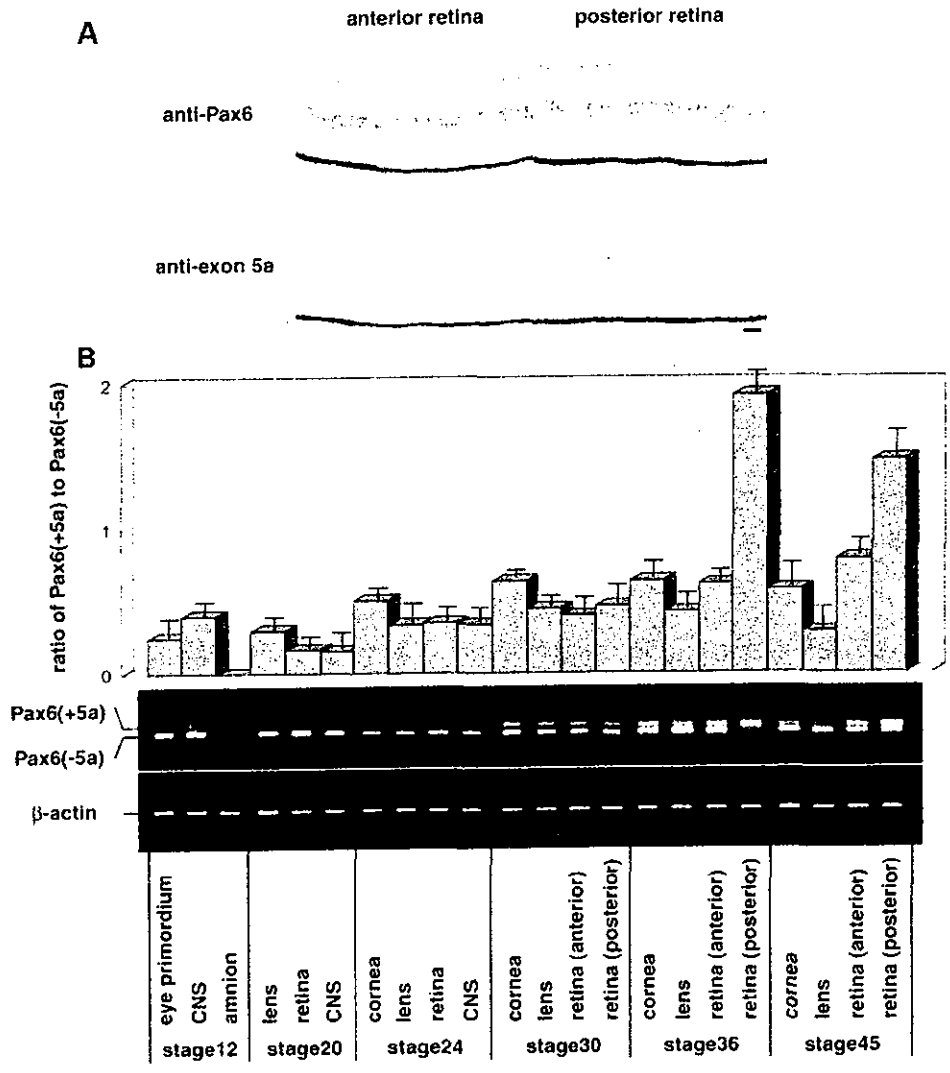

Figure 2. (A) Horizontal sections of the chick eye at HH stage 45 stained with anti-Pax6 or anti-exon 5a antibody (bar scale 20 μm). The Pax6(+5a) protein appears to localize in the posterior retina containing the visual streak, whereas the Pax6(−5a) protein distributes throughout the entire retina. (B) Semi-quantitative RT–PCR analysis of the expression of the two *Pax6* isoforms in developing chick embryos. As the eye became big enough to be dissected at later stages, *Pax6* expression could be examined in particular parts of the eye structure. The indicated PCR fragments were judged to represent one or the other *Pax6* isoform by their sizes. This was confirmed by sequencing. In the posterior retina, tissues were excised from the visual streak region. Amnion tissues were used as a negative control for *Pax6* expression and *β-actin* represents the amounts of RNA in each lane. The bar graph is shown as mean ± SD ($n = 3$) of expression ratio of Pax6(+5a) to Pax6(−5a). The photograph of RT–PCR analysis under the bar graph is representative of three independent experiments.

control eyes (Fig. 4A). Several isolated swelling spots (bulges) or lines (wrinkles) on the retina were observed in 68% of the 198 treated eyes. Green fluorescence was also observed at these areas (Fig. 4B). Histological examination showed that the retina was thickened and staining with anti-Islet1 and anti-neurofilament antibodies revealed that the differentiation of ganglion cells had expanded to the surface layer at these places (Fig. 4C). In 32% ($n = 198$) of the Pax6(−5a)-treated eyes, an embankment-like structure swelled out on the retina. In addition, several fibres (10–100 μm in length) grew out into the vitreous cavity (Fig. 4D). Sections were stained with specific antibodies for Islet1, a homeodomain-containing transcription factor that is expressed in the ganglion cells in the developing retina (30), and neurofilament protein, an intermediate filament protein specific to retinal neurons (31). The immunohistochemistry suggested that the fibres in the vitreous cavity were nerve bundles derived from ganglion cells (Fig. 4E). These abnormal structures may be caused by the unbalanced growth and differentiation of the retina, because the nerve fibres extended onto the retinal surface and formed additional layers on the retina.

When the Pax6(+5a) isoform was misexpressed instead of Pax6(−5a), more dramatic changes were observed inside the enlarged eyes 3–7 days after electroporation (HH stages 28–35). Of the 187 treated eyes, 6% had a wall-like structure protruding into the vitreous cavity, which was shown to be a

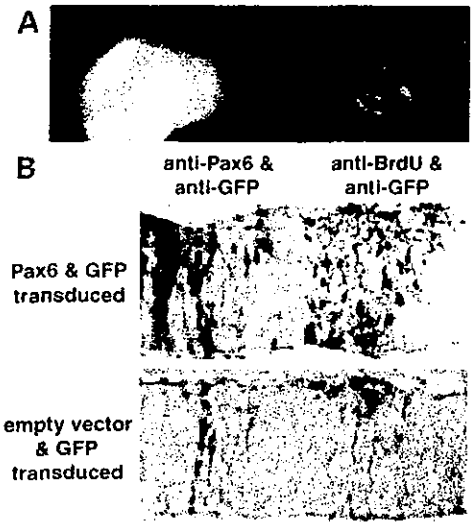

Figure 3. Early changes in the developing chick eye induced by the electroporation of Pax6(−5a). Constructs expressing Pax6(−5a) and GFP were electroporated into the right eye primordium of HH stage 16 chick embryos ($n = 5$). (**A**) Twelve hours after electroporation (HH stage 18), expression of GFP in the right eye was examined using fluorescence microscopy. (**B**) Sections double-immunostained with anti-GFP (violet) and anti-Pax6 (brown) and anti-GFP (violet) and anti-BrdU (brown) antibodies show the expression of the electroporated GFP and Pax6(−5a) constructs and the pronounced proliferation of the retinal progenitor cells around the electroporated area, but transduction of empty vector, pCAGGS-GFP or both constructs did not induce any change ($n = 5$ for each). (bar scale 20 μm). Transduction of the Pax6(+5a) isoform had a similar effect on eye development at these stages ($n = 5$; data not shown).

folded retina by histological analysis (Fig. 4G and H) and 42% showed thick stick-like structures protruding from the retina into the vitreous cavity (Fig. 4I and J). These protruding structures were very long and some even approached the lens on the opposite side. Cross sections of these protrusions were subjected to *in situ* hybridization with probes specific for *Musashi*, which encodes a neural RNA-binding protein highly enriched in neural precursor cells (32), *Six3*, a homologue of *Drosophila* homeobox gene *sine oculis*, that is expressed in inner and outer nuclear layers (33), and *Rx*, a paired-class homeobox gene, which is expressed in the inner nuclear layer, presumably bipolar cells of the developing retina (34). Immunohistochemical staining with anti-ISlet1 and anti-neurofilament antibodies was also performed (Fig. 4K). These analyses suggested that the tubular structures consist of well-differentiated retinal layers, which include nerve fibres, ganglion cells and developing inner and outer nuclear layer cells, with an outer surface layer of nerve fibres and an inner surface of photoreceptor cells. These tubular and fold structures suggest that the horizontal overgrowth of the neural retinal layer occurred at the regions where Pax6(+5a) was misexpressed. As space was limited even in the enlarged eyeball, the regional expansion of the cells seemed to push the retinal layer up into the vitreous cavity. Such drastic outgrowths that contain all retinal cell types was never obtained when Pax6(−5a) was misexpressed. Electroporation of the empty vector alone or the pCAGGS-GFP or both constructs did not induce any phenotypic changes. Thus, we conclude that the Pax6(+5a) isoform can induce horizontal overgrowths of the retina that protrude into the vitreous cavity. Of the 187 treated eyes, 34% of the Pax6(+5a)-treated eyes, which showed protrusion of the retina, became significantly larger than untreated control eyes (Fig. 4F). Although we have reproducibly generated this protruding retina by electroporating at HH stages 16–24, such morphological alterations were not induced when the electroporation was performed at later stages. Transduction of Pax6(−5a) or Pax6(+5a) using an adenoviral vector or electroporation using smaller amounts of plasmid DNAs caused similar, although somewhat weak phenotypic changes (data not shown). The incidence of the Pax6(−5a)- and Pax6(+5a)-dependent eye architectural changes at each stage is available in Supplementary Material.

We next examined the distribution of photoreceptor cells in the protruding retinal structures. Embryos were allowed to develop just before hatching (HH stages 40–45) and then analyzed. Some lectins, including peanut agglutinin and wheat germ agglutinin, specifically stain cone photoreceptor cells (35), which are normally condensed at the visual streak in the posterior portion of the chick eye (Fig. 5A and B e region). Histochemical examination revealed that the cone cells were detectable in the folded retina not only near the visual streak (d region) but also in the peripheral portion (c region) where lectin-staining is normally negative as observed in an unaffected peripheral portion (b region). Colour opsins are components of cone cells (2,3,36). RT–PCR showed that three types of colour *opsins* were expressed in the peripheral and posterior portions of the folded retina (c and d regions) at a similar level as in an unaffected region in the posterior portion of the retina (e region), and more intensely than an unaffected region of the peripheral portion of the retina (b region) (Fig. 5D). In contrast, the expression level of *rhodopsin*, a component of rod cells, was high in the peripheral areas and low in the visual streak (2,3). The peripheral portion of the folded retina (c region) exhibited *rhodopsin* expression at a similar level as the control peripheral area, whereas the expression level in the affected region in the posterior portion of the retina (d region) was similar to that in the visual streak (e region). These results suggest that the differentiation of retinal cells is highly promoted in the protruding retina to the level seen in the visual streak with regard to both the layer structure and the density of cone cells.

Effect of missense mutations of the *Pax6* gene on retinal overgrowth

To understand which element or structure of Pax6 is important for inducing the retinal overgrowth observed, we introduced several mutations into the Pax6 PD: (a) the R26G mutation in the NTS (25), (b) the R128C mutation in the CTS (4) or (c) the V54D mutation in exon 5a (5). The transactivation potentials of wild-type and mutant Pax6 with or without exon 5a have been assayed previously (5,22) or in this study using reporter genes containing P6CON or 5aCON, which are consensus binding sites for the (−5a) and (+5a) isoforms, respectively. As summarized in Figure 6A, the NTS in Pax6(−5a) wild-type is responsible for P6CON-binding,

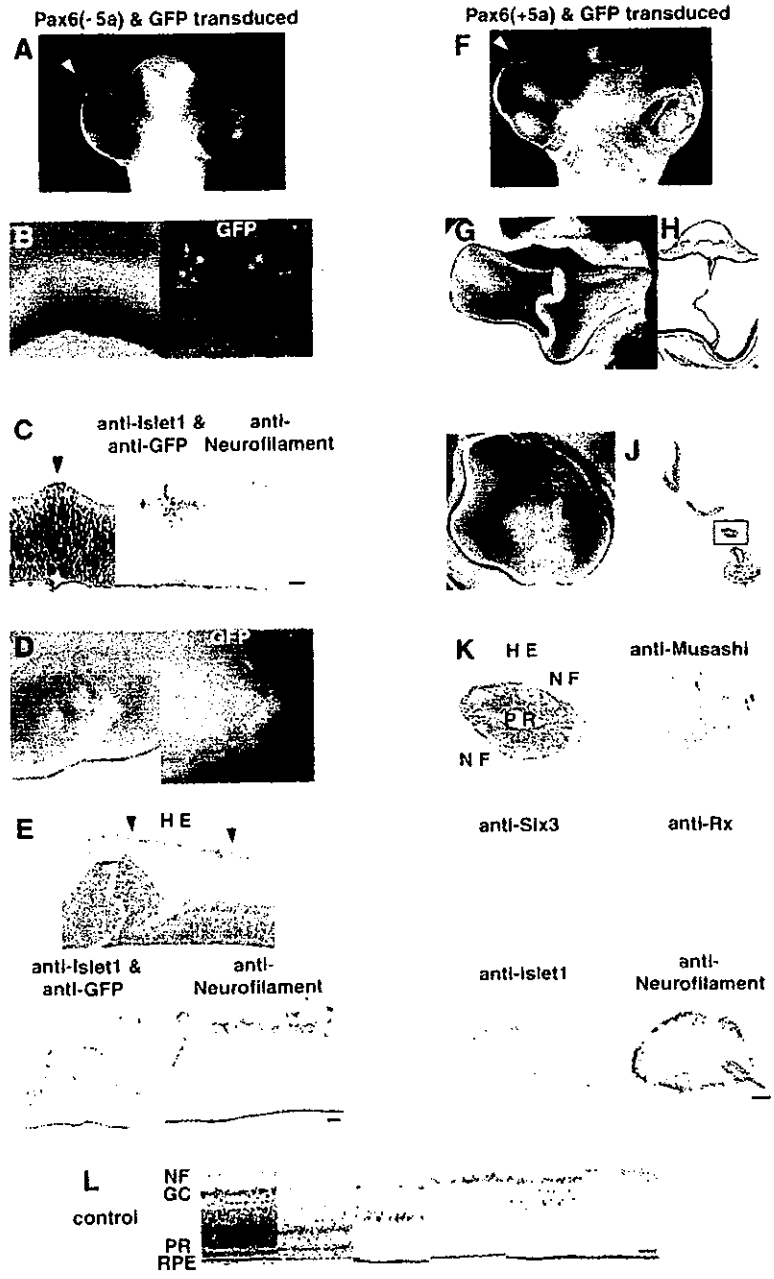

Figure 4. Later changes in the developing chick eye induced by electroporation of Pax6(−5a) (A–E) or Pax6(+5a) (F–K) together with GFP. (A–C) A Pax6(−5a)-transduced embryo at HH stage 30. (A) The frontal view shows an enlarged eye (arrowhead). (B) The inside views show several areas of swelling on the retinal layer with green fluorescence (the right panel, matched field). (C) Sections stained with HE, anti-islet1, anti-GFP and anti-neurofilament antibodies. Islet1 (brown) and GFP (violet) were double-stained. Ganglion cells (arrowhead) excessively differentiated in the surface layer of the thickened retina where the electroporated GFP constructs is expressed (bar scale 20 μm). (D, E) A Pax6(−5a)-transduced embryo at HH stage 34. (D) A view of the split eyeball shows embankment-like swelling from the retina with numerous fibres with green fluorescence (matched field). (E) Numerous fibres grow from the embankment-like retina into the vitreous cavity (arrowheads). Sections immunostained with anti-ISlet1 (brown), anti-GFP (violet in the left lower panel) and anti-neurofilament (brown) antibodies show expression of the electroporated constructs and ectopic growth of the nerve bundles from the retina (bar scale 20 μm). (F–H) A Pax6(+5a)-transduced embryo at HH stage 34. (F) A frontal view shows a significantly enlarged eye that breaks through the eyelid skin (arrowhead). Views of the split eyeball (G) and section with HE staining (H) show that the retina overgrows to show fold structure. (I–K) A Pax6(+5a)-transduced embryo at HH stage 36. Views of the split eyeball (I) and section with HE staining (J) show that the retina overgrows into stick structure. GFP expression was weak and could not be detected in the aberrantly growing tissues. (K) Analysis of the boxed region of the section indicated by (J) by *in situ* hybridization using probes specific for *Musashi*, *Six3* and *Rx* and immunohistochemistry with anti-islet1 and anti-neurofilament antibodies. These analyses suggest that the aberrantly growing tissues in the Pax6(+5a)-transduced eyes are composed of well-differentiated retina layers (bar scale 20 μm). NF, nerve fibres; PR, photoreceptors. (L) A portion of the posterior retina normally developing at a corresponding stage is illustrated for comparison. NF, nerve fibres; PR, photoreceptors; RPE, retinal pigment epithelium (bar scale 20 μm).

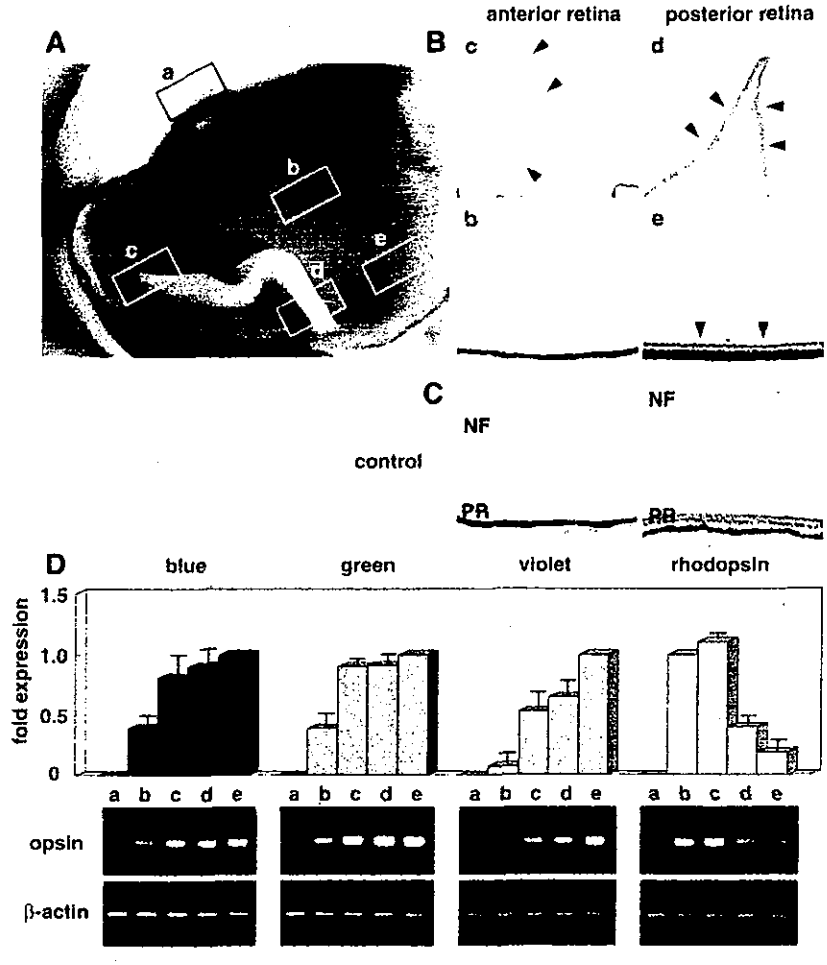

Figure 5. Differentiation of photoreceptor cells in the extruding and folded retina induced by electroporation of Pax6(+5a) at HH stage 18. (**A**) A view of a split eyeball at HH stage 45 shows the folded retina. Five areas were examined: (a) the cornea, (b) an unaffected region in the peripheral portion of the retina, (c) a peripheral portion of the folded retina, (d) a posterior portion of the folded retina and (e) an unaffected region in the posterior portion of the retina including the visual streak. (**B**) Staining with peanut agglutinin shows the presence of cone photoreceptor cells in the c region as well as in the d and e regions (arrowheads). (**C**) A portion of the retina normally developing at a corresponding stage is also illustrated for comparison. NF, nerve fibres; PR, photoreceptors (bar scale 20 μm). (**D**) Semi-quantitative RT–PCR demonstrates the expression of three colour *opsins* (*blue, green* and *violet*) and *rhodopsin* in the various regions. The bar graphs are shown as mean ± SD ($n = 3$) of ratio of expression in a–d region to that in e region (blue, green and violet *opsins*), or ratio of expression in a or c–e region to that in b region (*rhodopsin*). The photograph of RT–PCR analysis under the bar graph is representative of three independent experiments using six treated eyes.

while in Pax6(+5a) wild-type, the insertion of 14 amino acids encoded by exon 5a into the NTS abolishes its NTS P6CON-binding activity and unmasks the CTS 5aCON-binding ability. The R26G mutation in the NTS strongly impairs the NTS- and P6CON-mediated transcriptional activation of Pax6(−5a) and increases the CTS- and 5aCON-mediated transcriptional activation of Pax6(+5a). In contrast, the R128C mutation in the CTS abolishes the CTS- and 5aCON-mediated transcriptional activation of Pax6(+5a), and hyperactivates the NTS- and P6CON-mediated transcription activation of Pax6(−5a). The V54D mutation in exon 5a has a weak inhibitory effect on the CTS-and 5aCON-mediated transcriptional activation, but increases the NTS- and P6CON-mediated transcriptional activation. Thus, it has been proposed that the two subdomains negatively regulate each other, and exon 5a thus appears to function as a molecular switch that determines target gene specificity. When these mutants were misexpressed in the primordial retina of HH stages 16–30 chick embryos, only Pax6(+5a) R26G and Pax6(−5a) R128C induced a phenotypic change. Retinal overgrowth was observed in 34% and 26% of the eyes that had received Pax6(+5a) R26G ($n = 54$) and Pax6(−5a) R128C ($n = 56$) respectively, although the observed phenotypic changes were less significant than those induced by the respective wild-type Pax6 isoforms. Morphological changes induced by Pax6(+5a) R26G were more drastic than those induced by Pax6(−5a) R128C. Retinal swelling and string- and stick-like structures induced by Pax6(+5a) R26G (Fig. 6B), and fibres induced by Pax6(−5a) R128C (Fig. 6C) are shown as examples. The incidence of eye architectural changes by transduction of

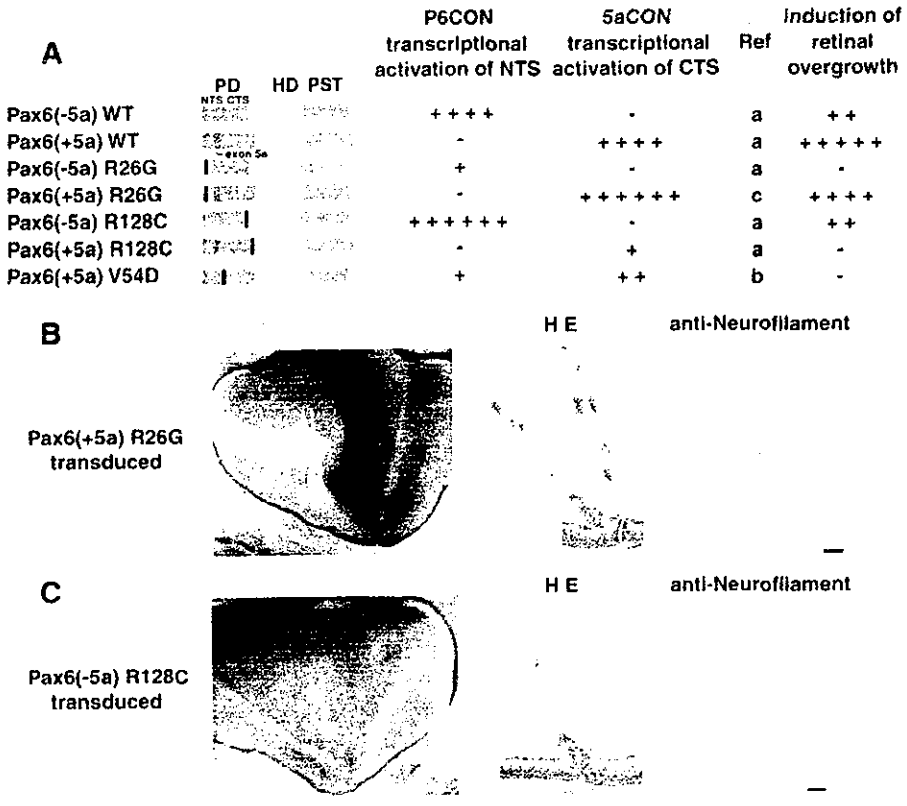

Figure 6. Effect of missense mutations of the *Pax6* gene on retinal overgrowth. (**A**) Schematic structure of the Pax6 wild-type and mutant (R26G, R128C and V54D) proteins with or without exon 5a that were used in this study. Our *in vitro* functional assays using P6CON- and 5aCON-CAT reporters in P19 cells have been reported previously [a, Yamaguchi *et al.* (22); b, Azuma *et al.* (5)] or are reported for the first time in this study (c). The effects of the mutants on overgrowth of the retina are also summarized. PD, paired domain (red, NTS; purple, CTS; blue, exon 5a; black bar, missense mutation); HD, homeodomain; PST, proline–serine–threonine rich transactivating domain. Each of the Pax6 mutants was electroporated into the right eye of HH stage 16 chick embryos and the changes around HH stage 35 were observed. (**B**) An eye that misexpresses Pax6(+5a) that carries the R26G mutation. The split eyeball shows the string- or stick-like structure of the overgrowing retina (left panel) (Pe, the pecten). Sections stained with HE and anti-neurofilament antibody suggest that the overgrowing tissues are thick bundles of nerve fibre and immature retina tissues (right panels, bar scale 100 μm). (**C**) An eye that misexpresses Pax6(−5a) that carries the R128C mutation. The split eyeball shows areas of swelling on the retina with fine fibres (left panel). Sections stained with HE and anti-neurofilament antibody reveal excessive differentiation of ganglion cells and their nerve fibres (right panels, bar scale 100 μm).

each mutant at each developmental stage is available in Supplementary Material.

DISCUSSION

We have shown here that when Pax6 is overexpressed in the developing chick eye, it induces ectopic differentiation of the retina. Compared with the effect of Pax6(−5a), Pax6(+5a) induces a remarkable artificial retina-like structure. Intriguingly, the ectopic retina-like structure induced by Pax6(+5a) is highly differentiated and contains well-formed retinal layers that express cone-specific colour opsins. We believe that the retinal overgrowth reported here is not an artifact but rather an exaggeration of the natural role of Pax6(+5a) in retinal development, namely, in the formation of the retinal area where visual cells highly accumulate. The assumption is based on two lines of evidence, as described subsequently.

First, Pax6(+5a) is expressed in a region of the developing retina where visual cells are densely packed (Figs 1 and 2). Previous studies have revealed that Pax6(+5a) is abundantly expressed in the lens and iris (37,38), but the expression pattern of Pax6(+5a) in the retina has not been clarified. As shown in previous studies and in the study reported here, the expression of the two Pax6 isoforms in the developing eye seems highly regulated at the levels of transcription and mRNA splicing (39,40).

Secondly, there is a clear correlation between the mutations in Pax6(+5a) that are associated with abnormal foveal formation in humans and that affect ectopic retinal formation in chick embryos. The V54D and R128C mutations disturbed the ectopic retinal structures induced by Pax6(+5a) as shown in Figure 6, while previous genetic analyses showed that these mutations are associated with foveal hypoplasia in human patients (4,5,26). As the V54D mutation in exon 5a should not affect the structure of Pax6(−5a), these observations suggest that Pax6(+5a) probably plays an important role in the formation of the fovea. Curiously, the V54D

mutation had only a modest effect on the transactivation activity of Pax6(+5a) in our reporter assay using P19 cells. It may be that a putative retina-specific cofactor that is not expressed in P19 cells may regulate the Pax6(+5a) activity in a V54D mutation-sensitive manner, thereby causing the apparent discrepancy. Alternatively, the V54D mutation may show a more potent effect when *cis* elements that diverge from the consensus sequences are used.

The two Pax6 isoforms seem to function differently in a qualitative rather than quantitative fashion. Pax6(−5a) overexpression does induce ectopic retina-like tissues. However, the incidence is far lower and the structures induced are far more immature when compared with those induced by Pax6(+5a) overexpression. As shown in Figure 6, the R26G mutation in the NTS and the R128C mutation in the CTS selectively impaired the induction of aberrant retinal structures by Pax6(−5a) and Pax6(+5a), respectively. Previous *in vitro* assays showed that Pax6(−5a) and Pax(+5a) bind to the distinct consensus sequences P6CON and 5aCON via different DNA-binding domains, namely, the NTS and the CTS, respectively. Thus, it is very likely that Pax6(−5a) and Pax6(+5a) have a different structural requirement for retinal development independently of each other and via different mechanisms. As these experiments were done in the retina that has endogenous Pax6 proteins, however, there is also a possibility that Pax6(+5a) exerts its effect on retinal development through modulation of Pax6(−5a) activity.

A different mechanism for Pax6-mediated gene regulation has been identified in *D. melanogaster* (41). There are four Pax6-related genes in *Drosophila*, namely *eyeless, twin of eyeless, eyegone* and *twin of eyegone*. Among them, *eyegone* has strong structural similarity with Pax6(+5a) and has been linked to growth control in the *Drosophila* eye. Overexpression of human Pax6(+5a) but not of Pax6(−5a) in *Drosophila* larvae induces strong overgrowth. Similarity of eyegone and Pax6(+5a) at a functional level is indicated by our data showing that overexpression of human Pax6(+5a) induces strong overgrowth of retina in the vertebrate eye.

Recently, mice lacking the Pax6(+5a) isoform were shown to have iris hypoplasia (38). Thus, the iris may be another part of the eye that is controlled by the Pax6(+5a) isoform. However, the knock-out mice showed no apparent abnormality in the retina. This does not conflict with our data, however, because mice intrinsically lack areas of high dense visual cells, including the fovea.

The regional expression of Pax6(+5a) may also be related to eyeball structure. It has been reported that a strictly controlled level of Pax6 expression is critical for the normal development of eyes. Transgenic mice carrying multiple copies of the Pax6 gene manifest severe eye anomalies and microphthalmos (42), while the same abnormalities are observed in mice with haploinsufficiency of this gene (43). However, microphthalmos is often associated with eye anomalies in which numerous eye tissues are affected (44,45). As Pax6 is expressed in numerous eye tissues throughout development (15–17), it may be that in the transgenic mice, the eye tissues, each of which expresses an abnormal dose of the gene (either loss-of-function or gain-of-function), affect neighbouring tissues and disturb their mutual relationship in eyeball growth, resulting in microphthalmos. In contrast, *in ovo* electroporation is able to transfer genes to a selected tissue. In our experiment, overexpression of Pax6 in the chick retina primordium caused enlarged eyes. The outer coat of the eyeball corresponding to areas of Pax6(+5a) misexpression was prominently enlarged. It is thought that retinal growth influences eyeball growth (1,45), and that the accumulation of retinal cells in the temporal posterior area may cause a larger growth in the temporal side of the eyeball than in the nasal side. Regional expression of the Pax6(+5a) isoform in the temporal posterior retina may lead to eyeball asymmetry.

Our observations also have implications regarding phylogenic development. The retinal layer structures are much more complex in vertebrates than in invertebrates. Structures that caused the visual cells to congregate at high density, such as the fovea, area centralis and visual streak, and eyeball asymmetry first appeared in fishes (1–3). The splice variant of Pax6 with exon 5a is present in vertebrates but not in invertebrates (20,21,38) except for *Drosophila*, which has *eyegone*, a putative homologue of Pax6(+5a) (42). Therefore, the acquisition of the Pax6 splice variant during evolution may have contributed to the formation of highly organized eye architectures that yield better vision. Thereafter, vertebrates may have preserved exon 5a so that they could form a restricted retinal domain that has high visual acuity.

The mechanism that regulates Pax6 alternative splicing has not yet been elucidated. Areas where retinal cells accumulate, including the visual streak, area centralis, and fovea, are positioned to promote visual acuity among animal species. Thus, further studies should focus on the signalling molecules that regulate the expression of Pax6 isoforms. In reproductive medicine research, studies have focused on transferring transcriptional factors into stem cells (46). As Pax6 induces the ectopic formation of eyes in flies (13) and frogs (14), this gene may be useful for regenerating regional eye tissue in vertebrates as well. Our results indicate that the use of Pax6(+5a) may be more suitable than Pax6(−5a) for reproducing highly differentiated retinal structures.

MATERIALS AND METHODS

Immunohistochemistry and *in situ* hybridization

A monoclonal antibody against chicken Pax6 that reacts to both Pax6(−5a) and Pax6(+5a) in chicken, monkey and human tissues has been described previously (16,17). A polyclonal antibody against the 14 amino acid residues encoded by exon 5a (THADAKVQVLDNQN) was raised by immunizing New Zealand white rabbits with a synthetic peptide. After purification, the immunoreactivity of the antibody was confirmed by ELISA and its specificity was further assayed by western blotting (data not shown). Antibodies against GFP (Clontech), 5-bromo-2′-deoxyuridine (BrdU; DAKO), Islet-1 protein (DSHB), Chx10 protein (Exalpha Biologicals), neurofilament H (DAKO) and peanut agglutinin (Vector) were purchased. Specimens were fixed in 4% paraformaldehyde, embedded in a Tissue-Tek OCT compound (Sankyo, Tokyo), and cryo-sliced into 8 μm sections. The sections were stained with haematoxylin and eosin (HE), or with a specific antibody followed by visualization with peroxydase

and diaminobenzidine. Section *in situ* hybridization was performed as described (47). Probes were prepared from plasmids that contain chick *Musashi* (*Eco*RI, *T7* polymerase), *Six3* (*Hin*dIII, *T3*) and *Rx* (*Hin*dIII, *T3*).

RNA isolation and RT–PCR

Total RNA was isolated from tissues excised from one to five chick embryos using an RNeasy Mini Kit (Qiagen) and converted to cDNA by a standard procedure using SuperScript II reverse transcriptase and adapter primers (GibcoBRL). cDNA was amplified under nonsaturating PCR conditions using the following primer sets: chicken *Pax6*, 5′-CGGCAG AAGATCGTGGAACTCG and 5′-GCACTCTCGTTTATA CTGCGCTAT [this yields a 207 bp band for *Pax6(−5a)* and a 249 bp band for *Pax6(+5a)*]; chicken *blue opsin*, 5′-GGCCTTTATGTTCCTCCTCATCG and 5′-CAGATGA CGAGGAAGCGCTCGA (297 bp); *green opsin*, 5′-TCCCT GGTGGTCTTGGCCATAG and 5′-TGCCTCTCGGACTTT GCAGATGA (320 bp); *violet opsin*, 5′-CTACCTACAG ACGGCCTTCATG and 5′-GCAGATAACGATGTAACG CTCGA (310 bp); and *rhodopsin*, 5′-GGCTGCCTACAT GTTCATGCTGA and 5′-ACGGCCAGGACGACGAGT GAC (281 bp). The PCR products were separated by gel electrophoresis. To standardize the RNA amounts, *β-actin* was also amplified by PCR with its specific primers: 5′-GT GGGTCGCCCCAGACATCA and 5′-CTCCTTGATGTCAC GCACAATTTC (540 bp). The PCR amplication involved 30 cycles of 94°C for 1 min, 60°C for 1 min and 72°C for 2 min. It should be noted that the alternative splicing exon of the human and mouse *Pax6* genes is situated between exon 5 and 6 and is known as 5a. However, the *Pax6* gene structure of the chick strain we used has not yet been fully determined. It may be that the alternative splicing exon of the chick may later be designated differently. For example, it has been suggested that this exon in the quail *Pax6* gene should be denoted as exon 4a. Nevertheless, in this report, we employ the term 5a to indicate the alternative splicing exon in the chick *Pax6* gene.

In ovo electroporation

Expression plasmids [pCAGGS-PAX6(−5a) and pCAGGS-PAX6(+5a)] carry the entire human *PAX6* coding region with or without exon 5a under the control of a cytomegalovirus enhancer and chicken β-actin promoter (5,22). The mutant forms of PAX6 expression plasmid were generated by PCR-based *in vitro* mutagenesis (5,22,27). Fertilized eggs of a domestic chick strain were purchased from Nisseizai (Tokyo). A small window was opened for access, and phosphate buffered saline was poured over the embryo to obtain appropriate resistance. The eggs were injected with ~0.1 μl of the DNA solution that contains an expression construct for GFP (pCAGGS–GFP) and one of the Pax6 expression plasmids (5 mg/ml) together with a fastgreen dye. The dye confirms that the injection was correctly targeted. Eggs, in which early changes are examined, were also injected with BrdU (0.3 mg/ml). The DNA solution was either injected into a region that is close to the primitive retina in the right optic cup or directly into the retina of the right eye of the embryos with a sharp glass pipette. The head of the embryo was then placed between platinum electrodes and electric pulses were applied (25–40 V, 90 ms, one to six times) with a CUY 21 electroporator (BEX Co., Tokyo). The egg-shells were sealed and the embryos were allowed to develop in humidified incubators at 38°C.

SUPPLEMENTARY MATERIAL

Supplementary Material is available at HMG Online.

ACKNOWLEDGEMENTS

We thank Drs H. Fujisawa (Nagoya University) and Y. Tanioka (Central Institute for Experimental Animals) for providing antibodies and marmoset specimens, respectively. We also thank Ms K. Saito for manuscript preparation. This study was supported in part by Grants for Genome, Tissue Engineering Biotechnology, for Sensory and Communicative Disorders, and for Paediatric Researches from the Ministry of Health, Labour and Welfare, Japan, and in part by a Grant for Organized Research Combination System from the Ministry of Education, Culture, Sports, Science and Technology, Japan.

REFERENCES

1. Duke-Elder, S. (1958) The eye in evolution. In *System of Ophthalmology*, Henry Kimpton, London, Vol. 1. Q2
2. Rodieck, R.W. (1998) *The First Step of Seeing*. Sinauer, Sunderland.
3. Oyster, C.W. (1999) *The Human Eye*. Sinauer, Sunderland.
4. Azuma, N., *Nishina*, S., Okuyama, T., Yanagisawa, H. and Yamada, M. (1996) PAX6 missense mutation in isolated foveal hypoplasia. *Nat. Genet.*, **13**, 141–142.
5. Azuma, N., Yamaguchi, Y., Handa, H., Hayakawa, M., Kanai, A. and Yamada, M. (1999) Missense mutation in the alternative splice region of the *PAX6* gene in eye anomalies. *Am. J. Hum. Genet.*, **65**, 656–663.
6. McCabe, K.L., Gunther, E.C. and Reh, T.A. (1999) The development of the pattern of retinal ganglion cells in the chick retina: mechanisms that control differentiation. *Development*, **126**, 5713–5724.
7. Marquardt, T., Ashery-Pedan, R., Andrejewski, N., Scardigli, R., Guillemot, F. and Gruss, P. (2001) Pax6 is required for the multipotent state of retinal progenitor cells. *Cell*, **105**, 43–55.
8. Sharon, D., Blackshaw, S., Cepko, C.L. and Dryja, T.P. (2002) Profile of the genes expressed in the human peripheral retina, macula, and retinal pigment epithelium determined through serial analysis of gene expression (SAGE). *Proc. Natl Acad. Sci. USA*, **99**, 315–320.
9. Gehring, W.J. (1996) The master control gene for morphogenesis and evolution of the eye. *Genes Cells*, **1**, 11–15.
10. Callaerts, P., Halder, G. and Gehring, W.J. (1997) PAX-6 in development and evolution. *Annu. Rev. Neurosci.*, **20**, 483–532.
11. Ashery-Padan, R. and Gruss, P. (2001) Pax6 lights-up the way for eye development. *Curr. Opin. Cell Biol.*, **13**, 706–714.
12. Chi, N. and Epstein, J.A. (2002) Getting your Pax straight: Pax proteins in development and disease. *Trends Genet.*, **18**, 41–47.
13. Halder, G., Callaerts, P. and Gehring, W.J. (1995) Induction of ectopic eye by targeted expression of the eyeless gene in *Drosophila*. *Science*, **267**, 1788–1792.
14. Chow, R.L., *Altmann*, C.R., Lang, R.A. and Hemmati-Brivanlou, A. (1999) *Pax6* induces ectopic eye in a vertebrate. *Development*, **126**, 4213–4222.
15. Walther, C. and Gruss, P. (1991) *Pax6*, a murine paired box gene, is expressed in the developing CNS. *Development*, **113**, 1435–1449.
16. Kawakami, A., Kimura-Kawakami, M., Nomura, T. and Fujisawa. H. (1997) Distributions of PAX6 and PAX7 proteins suggest their involvement in both early and late phases of chick brain development. *Mech. Dev.*, **66**, 119–130.

17. Nishina, S. Kohsaka, S., Yamaguchi, Y., Handa, H., Kawakami, A., Fujisawa, H. and Azuma, N. (1999) PAX6 expression in the developing human eye. *Br. J. Ophthalmol.*, **83**, 723–727.
18. Czerny, T., Schaffner, G. and Busslinger, M. (1993) DNA sequence recognition by Pax proteins: bipartite structure of the paired domain and its binding site. *Genes Dev.*, **7**, 2048–2061.
19. Xu, W., Rould, M.A., Jun, S., Despan, C. and Pabo, C.O. (1995) Crystal structure of a paired domain-DNA complex at 25A resolution reveals structural basis for Pax developmental mutations. *Cell*, **80**, 639–650.
20. Epstein, J.A., Glaser, T., Cai, J., Jepeal, L., Walton, D.S. and Maas, R.L. (1994) Two independent and interactive DNA-binding subdomains of the Pax6 paired domain are regulated by alternative splicing. *Genes Dev.*, **8**, 2022–2034.
21. Epstein, J.A., Cai, J., Glaser, T., Jepeal, L. and Maas, R.L. (1994) Identification of a Pax paired domain recognition sequence and evidence for DNA-dependent conformational changes. *J. Biol. Chem.*, **269**, 8355–8361.
22. Yamaguchi, Y., Sawada, J., Yamada, M., Handa, H. and Azuma, N. (1997) Autoregulation of Pax6 transcriptional activation by two distinct DNA-binding subdomains of the paired domain. *Genes Cells*, **2**, 255–261.
23. Richardson, J., Cvekl, A. and Wistow, G. (1995) Pax-6 is essential for lens-specific expression of zeta-crystallin. *Proc. Natl Acad. Sci. USA*, **92**, 4676–4680.
24. Martha, A., Ferrell, R.E., Mintz-Hittner, H., Lyons, L.A. and Saunders, G.F. (1994) Paired box mutations in familial and sporadic aniridia predicts truncated aniridia proteins. *Am. J. Hum. Genet.*, **54**, 801–811.
25. Hanson, I., Fletcher, J.M., Jordan, T., Brown, A., Taylor, D., Adams, R.J., Punnett, H.H. and van Heyningen, V. (1994) Mutations at the *PAX6* locus are found in heterogeneous anterior segment malformations including Peters' anomaly. *Nat. Genet.*, **6**, 168–173.
26. van Heyningen, V. and Williamson, K.A. (2002) PAX6 in sensory development. *Hum. Mol. Genet.*, **11**, 1161–1167.
27. Azuma, N., Yamaguchi, Y., Handa, H., Tadokoro, K., Asaka, A., Kawase. E. and Yamada, M. (2003) Mutations of the *PAX6* gene detected in patients with a variety of optic nerve malformations. *Am. J. Hum. Genet.*, **72**, 1565–1570.
28. Itasaki, N., Bel-Vialar, S. and Krumlauf, R. (1999) 'Shocking' developments in chick embryology: electroporation and *in ovo* gene expression. *Nat. Cell Biol.*, **1**, E203–207.
29. Niwa, H., Inoue, S., Hirano, T., Matsuo, T., Kojima, S., Kubota, M., Ohashi, M. and Tsuji, F.I. (1996) Chemical nature of the light emitter of the Aequorea green fluorescent protein. *Proc. Natl Acad. Sci. USA*, **93**, 13617–13622.
30. Halfter, W. (1998) Disruption of the retinal basal lamina during early embryonic development leads to a retraction of vitreal end feet, an increased number of ganglion cells, and aberrant axonal outgrowth. *J. Comp. Neurol.*, **397**, 89–104.
31. Torelli, S., Sogos, V., Marzilli, M.A., D'Atri, M. and Gremo, F. (1989) Developmental expression of intermediate filament proteins in the chick embryo retina: *in vivo* and *in vitro* comparison. *Exp. Biol.*, **48**, 187–196.
32. Sakakibara, S. and Okano, H. (1997) Expression of neural RNA-binding proteins in the postnatal CNS: implications of their roles in neuronal and glial cell development. *J. Neurosci.*, **17**, 8300–8312.
33. Kawakami, K., Ohto, H., Takizawa, T. and Saito, T. (1996) Identification and expression of six family genes in mouse retina. *FEBS Lett.*, **393**, 259–263.
34. Mathers, P.H., Grinberg, A., Mahon, K.A. and Jamrich, M. (1997) The *Rx* homeobox gene is essential for vertebrate eye development. *Nature*, **387**, 603–607.
35. Hageman, G.S. and Kuehn, M.H. (1998) Biology of the interphotoreceptor matrix–retinal pigment epithelium–retina interface. In Marmor, M. and Wolfensberger, T.J. (eds), *The Retinal Pigment Epithelium*. Oxford University Press, New York, pp. 361–391.
36. Nathans, J., Thomas, D. and Hogness, D.S. (1986) Molecular genetics of human color vision: the gene encoding blue, green, and red pigments. *Science*, **232**, 193–202.
37. Jaworski, C., Sperbeck, S., Graham, C. and Wistow, G. (1997) Alternative splicing of Pax6 in bovine eye and evolutionary conservation of intron sequences. *Biochem. Biophys. Res. Commun.*, **240**, 196–202.
38. Singh, S., Mishra, R., Arango, N.A., Deng, J.M., Behringer, R.R. and Saunders, G.F. (2002) Iris hypoplasia in mice that lack the alternatively spliced Pax6(5a) isoform. *Proc. Natl Acad. Sci. USA*, **99**, 6812–6815.
39. Kumar, J.P. (2001) Signalling pathways in *Drosophila* and vertebrate retinal development. *Nat. Rev. Genet.*, **2**, 846–857.
40. Marquardt, T. and Gruss P. (2002) Generating neuronal diversity in the retina: one for all. *Trends Neurosci.*, **25**, 32–38.
41. Dominguez, M., Ferres-Marco, D., Gutierrez-Avino, F.J., Speicher, S.A. and Beneyto, M. (2004) Growth and specification of the eye are controlled independently by eyegone and eyeless in *Drosophila melanogaster*. *Nat. Genet.*, **36**, 31–39.
42. Schedl, A., Ross, A., Lee, M., Engelkamp, D., Rashbass, P., van Heyningen, V. and Hastie, N.D. (1996) Influence of *PAX6* gene dosage on development: overexpression causes severe eye abnormalities. *Cell*, **86**, 71–82.
43. Hill, R.E., Favor, J., Hogan, B.L., Ton, C.C., Saunders, G.F., Hanson, I.M., Prosser, J., Jordan, T., Hastie, N.D. and van Heyningen, V. (1991) Mouse small eye results from mutations in a paired-like homeobox-containing gene. *Nature*, **354**, 522–525.
44. Duke-Elder, S. (1964) Congenital deformities. In *System of Ophthalmology*, Henry Kimpton, London, Vol. 3, part 2.
45. Burmeister, M., Novak, J., Liang, M.Y., Basu, S., Ploder, L., Hawes, N.L., Vidgen, D., Hoover, F., Goldman, D., Kalnins, V.I. *et al.* (1996) Ocular retardation mouse caused by Chx10 homeobox null allele: impaired retinal progenitor proliferation and bipolar cell differentiation. *Nat. Genet.*, **12**, 376–384.
46. Haruta, M., Kosaka, M., Kanegae, Y., Saito, I., Inoue, T., Kageyama, R., Nishida, A., Honda, Y. and Takahashi, M. (2001) Induction of photoreceptor-specific phenotypes in adult mammalian iris tissue. *Nat. Neurosci.*, **4**, 1163–1164.
47. Koshiba-Takeuchi, K., Takeuchi, J.K., Matsumoto, K., Momose, T., Uno, K., Hoepker, V., Ogura, K., Takahashi, N., Nakamura, H., Yasuda, K. *et al.* (2000) Tbx5 and the retinotectum projection. *Science*, **287**, 134–137.

Human Molecular Genetics, 2005, Vol. 14, No. 8 1–10
doi:10.1093/hmg/ddi098
Advance Access published on xxx

Transdifferentiation of the retinal pigment epithelia to the neural retina by transfer of the Pax6 transcriptional factor

Noriyuki Azuma[1,2,*], Keiko Tadokoro[2], Astuko Asaka[2], Masao Yamada[2], Yuki Yamaguchi[3], Hiroshi Handa[3], Satsuki Matsushima[4], Takashi Watanabe[4], Yasuyuki Kida[5], Toshihiko Ogura[5], Kenji Shimamura[6,7] and Masato Nakafuku[6,8]

[1]Department of Ophthalmology, National Center for Child Health and Development, Tokyo 157-8535, Japan, [2]Department of Genetics, National Research Institute for Child Health and Development, Tokyo 154-8567, Japan, [3]Department of Biological Information, Tokyo Institute of Technology, Graduate School of Bioscience and Biotechnology, Yokohama, 226-8501, Japan, [4]Department of Clinical Research Medicine, Kyorin University School of Medicine, Tokyo 181-8611, Japan, [5]Department of Developmental Neurobiology, Institute of Development, Aging and Cancer, Sendai 980-8575, Japan, [6]Department of Neuroscience, University of Tokyo Graduate School of Medicine, Tokyo 113-0033, Japan, [7]Division of Morphogenesis, Department of Embryogenesis, Institute of Molecular Embryology and Genetics, Kumamoto University, Honjo 2-2-1, Kumamoto 860-0811, Japan and [8]Division of Developmental Biology, Cincinnati Children's Hospital Research Foundation, Cincinnati, OH 45229, USA

Received December 19, 2004; Revised and Accepted March 2, 2005

The *Pax6* gene plays an important role in eye morphogenesis throughout the animal kingdom. The *Pax6* gene and its homologue could form ectopic eyes by targeted expression in *Drosophila* and *Xenopus*. Thus, this gene is a master gene for the eye morphogenesis at least in these animals. In the early development of the vertebrate eye, Pax6 is required for the instruction of multipotential progenitor cells of the neural retina (NR). Primitive retinal pigment epithelial (RPE) cells are able to switch their phenotype and differentiate into NR under exogenous intervention, including treatment with fibroblast growth factors (FGFs), and surgical removal of endogenous NR. However, the molecular basis of phenotypic switching is still controversial. Here, we show that Pax6 alone is sufficient to induce transdifferentiation of ectopic NR from RPE cells without addition of FGFs or surgical manipulation. Pax6-mediated transdifferentiation can be induced even at later stages of development. Both *in vivo* and *in vitro* studies show that the Pax6 lies downstream of FGF signaling, highlighting the central roles of Pax6 in NR transdifferentiation. Our results provide an evidence of retinogenic potential of nearly mature RPE and a cue for new therapeutic approaches to regenerate functional NR in patients with a visual loss.

INTRODUCTION

Once the neural retina (NR) is damaged by developmental malformation or age-related degeneration, it is unable to regenerate, therefore resulting in a significant visual loss. Regeneration of well-defined NR has not been induced in human retinal tissues by previous trials. In contrast, in adult salamander eyes, fully functional NR regenerates from retinal pigment epithelial (RPE) cells, when the endogenous NR is surgically removed (1). However, this regenerative event can be seen only in some amphibian eyes, but not in the eyes of other higher animals. Nonetheless, Muller cells in the postnatal chick NR de-differentiate and form NR neurons, in response to acute chemical damage (2). Pigmented ciliary margin cells in the adult mouse eye are able to form sphere colonies *in vitro* and differentiate into NR specific

*To whom correspondence should be addressed at: Department of Ophthalmology, National Center for Child Health and Development, 2-10-1, Okura, Seatagaya-ku, Tokyo 157-8535, Japan. Tel: +81 334160181; Fax: 81 334162222; Email: azuma-n@ncchd.go.jp

cells, including photoreceptors (PR), bipolar cells and Muller cells (3). Iris tissues in the adult rat eye generate cells expressing rhodopsin, a specific antigen for rod PR (4). These observations suggest that, even in higher animals, regeneration of functional NR could be induced in some circumstances.

In embryonic eyes of chicks and mice, the primitive RPE (until embryonic day 4.5 in chick embryos, and E15 in rat embryos) is able to switch its phenotype and transdifferentiate into NR when treated with fibroblast growth factors (FGFs) (5–8). The two distinct functional components of the vertebrate retina, the inner NR and outer RPE, develop as a two-layered optic cup that is formed by folding the optic vesicle at an early stage of development. Because FGFs are expressed in the anterior parts of the primitive eye, they are considered to play roles for NR differentiation as well (6). Primitive RPE may still have retinogenic potential, but once it differentiates to mature one, it loses its potential to transdifferentiate to NR even by treatment with FGFs. Although several transcription factors and signaling cascade have been reported to act downstream of FGF signaling (7,8), nuclear events that control the differentiation competence of FGF signaling remain unsolved.

The *Pax6* gene, encoding a paired-class transcription factor, is critical for eye development (9). Target expression of the *eyeless* gene, a *Pax6* homologue of *Drosophila melanogaster*, results in ectopic formation of functional compound eyes on the wings, legs and antennae (10). The *Pax6* can also induce ectopic eyes in frog *Xenopus larvae* (11), indicating that the gene can initiate the regulatory cascade for eye formation in both invertebrates and vertebrates. Ectopic eyes in frogs contain all major components of eye, but not the full architecture. Ectopic eye architectures have been also induced by misexpression of other transcription factors, *eyes absent* (12–14), *sine oculis/Six*(14–18), *dachshund* (13,19), *Rx* (20) and *teashirt*(21), that lie downstream of or cooperate with *eyeless/Pax6* in the eye morphogenesis, in *Drosophila* (12–14,19,21) and vertebrates (15–18,20). However, such ectopic eye architectures are far smaller and more immature compared with those induced by *eyeless/Pax6* misexpression. Thus, *Pax6* could be a useful tool for the regeneration of eye tissues in vertebrates. We transduced the human *Pax6* gene into avian RPE cells *in vivo*, and elucidate here a direct role of the *Pax6* gene in transdifferentiation of fully structured NR from nearly mature RPE cells and also a functional relationship between FGF signaling and this gene.

RESULTS

In ovo misexpression of the *Pax6* gene induces fully structured NR from RPE cells

To analyze the effect of Pax6 on RPE, expression plasmids that carry the human *Pax6* cDNAs were misexpressed in the RPE of chick embryos by *in ovo* electroporation (22). The *Pax6* gene produces two isoforms by alternative splicing: one with exon 5a and another without this exon. The variant 5a form has an additional 14 amino acid residues inserted into the DNA-binding domain, paired domain (PD) (23,24). We generated two plasmids carrying each isoform [pCAGGS–Pax6(−5a) or pCAGGS–Pax6(+5a)] (25–27). Areas expressing the exogenous gene were monitored by signals of green fluorescence protein (GFP) by co-electroporating pCAGGS–GFP (Fig. 1A) (28).

When Pax6(−5a) or Pax6(+5a) was misexpressed in the RPE at stage 12–40, RPE cells were found to lose their intracellular pigments and form a thick cell layer 1–2 days after electroporation, whereas the control RPE, in which empty plasmid (pCAGGS) alone, pCAGGS–GFP or both constructs were electroporated, showed the normal morphology. Immunohistochemical analyses using anti-GFP and anti-Pax6 antibodies detected distinct staining in the thickened RPE layer. Cross sections were subjected to *in situ* hybridization with probes specific for transcription factors or signaling molecules that regulate the proliferation of retinal progenitor cells and the specification of cell fate. *Musashi*, which encodes a neural RNA-binding protein, highly enriched in neural precursor cells (29). *Notch1*, which encodes a receptor for a signaling pathway, regulates neurogenesis (30). *Six3*, a homologue of *Drosophila* homeobox gene *sine oculis*, is early on expressed in the optic vesicle, turns off in the future pigment epithelium and becomes restricted to the prospective NR and to the lens placode. In the NR development, *Six3* is expressed in the entire undifferentiated neuroepithelium, then in differentiating cell layers including the inner and outer nuclear layer, and ganglion cell layer (31). *Rx*, a paired-class homeobox gene, is expressed early on in the optic vesicle and later on in the inner on nuclear layer, presumably bipolar cells of the developing NR (20). *In situ* hybridization detected signals for *Musashi*, *Notch1* and *Rx* 12 h after electroporation (Fig. 1B), then that for *Six3* 36 h after electroporation (Fig. 1C), suggesting that they transdifferentiate to NR. Signals for *Rx* in endogenous and ectopic retinas transiently decreased at a stage when bipolar cells do not yet differentiate. At these early phases post-*Pax6* transduction, immunohistochemical staining with antibodies against retinal cell markers cited below was yet undetectable (data not shown). When electroporation was performed even in stage 40 embryos, RPE cells were still found to transdifferentiate to NR. GFP fluorescence is no longer detectable 5–7 days after electroporation, as expression of GFP was terminated or faded out owing to cell growth. In a serial section of each eye at early phases after electroporation, NR transdifferentiation was seen only within the areas showing GFP fluorescence. Electroporation of the pCAGGS alone, pCAGGS–GFP or both constructs failed to induce transdifferentiation, suggesting that the *Pax6* gene alone is able to transdifferentiate NR from RPE cells without addition of FGFs or surgical manipulation. Embryos were unable to survive or hatch, when electroporation was performed at later than stage 40.

Four to five days after electroporation, formation of ectopic NR occurred as a wide sheet, but later in spotted areas, which scattered in the whole fundus (Fig. 2A). Sections showed that the ectopic NR is well differentiated, and the vertical direction of the transdifferentiated NR layers was reversed with PR inside and ganglion cells outside (Fig. 2B), similar to the FGF-treated eyes (5–8). Cross sections were subjected to *in situ* hybridization with probes specific for *Musashi*, *Notch1*, *Six3* and *Rx*. Sections also were subjected to immunohistochemistry with antibodies against retinal cell markers: Islet1, a homeodomain-containing transcription factor that is

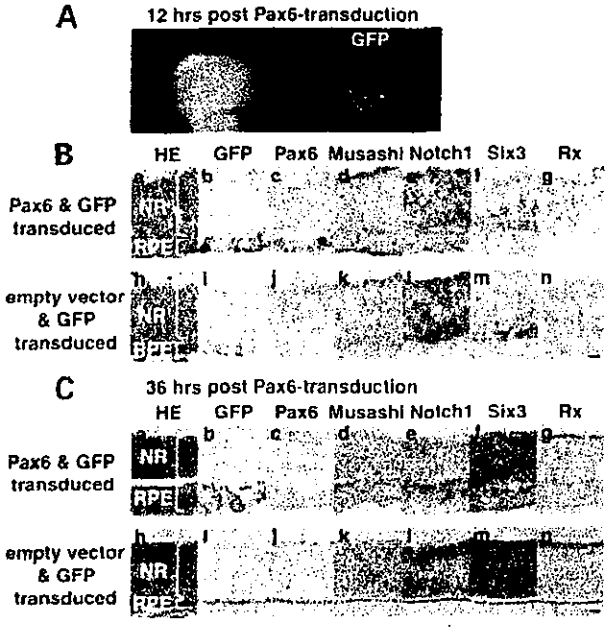

Figure 1. Early phases of NR transdifferentiation from RPE cells by electroporation of the *Pax6* gene. The *Pax6* and *GFP* genes were misexpressed into the outer layer of the optic cup of stage 18 chick embryos. Eyes were examined 12 h (**A** and **B**) and 36 h (**C**) after electroporation. (A) Expression of GFP in the outer layer of the right eye was examined using fluorescence microscopy. (B and C) Light microscopy [a, h; hematoxylin and eosin (HE) staining]. Immunohistochemistry with antibodies for GFP (b, i) and Pax6 (c, j). *In situ* hybridization with probes specific for *Musashi* (d, k), *Notch1* (e, l), *Six3* (f, m) and *Rx* (g, n). Eyes misexpressed with Pax6 (a–g) and controls (h–n). Pax6 in the thickened RPE layer are exogenous, whereas that in NR may be endogenous (c). Bars, 20 μm.

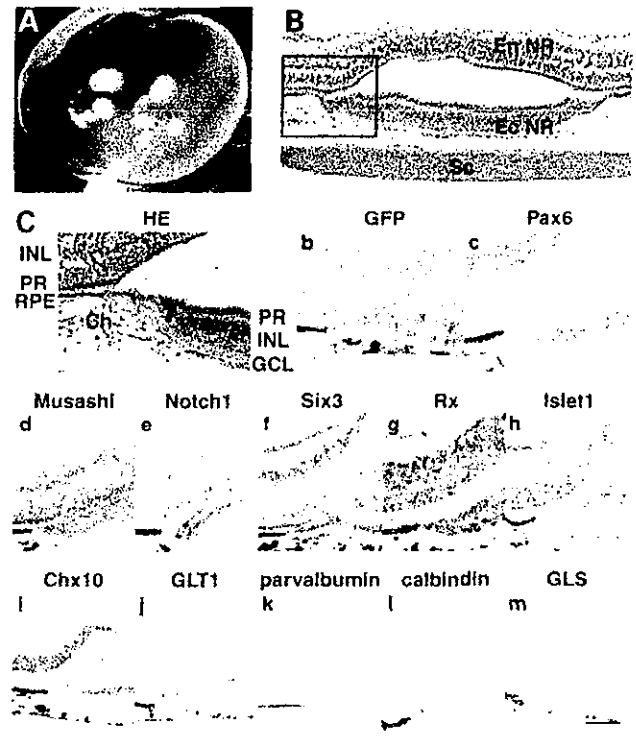

Figure 2. Fully structured NR transdifferentiation from RPE cells by electroporation of the *Pax6* gene. The *Pax6* gene was misexpressed into the RPE layer of stage 24 chick embryos, and eyes were examined at stage 40. (**A**) In a half of the eyeball, patched areas of white swelling tissue are scattered. At this time, GFP is no longer detectable by fluorescence microscopy (data not shown). (**B**) Light microscopy [hematoxylin and eosin (HE) staining] of the white swelling tissue in (A). EcNR, the ectopic NR transdifferentiated from RPE; EnNR, the endogenous NR; Sc, the sclera. (**C**) Light microscopy (a; HE staining), immunohistochemistry with antibodies for GFP (b), Pax6 (c), Islet1 (h), Chx10 (i), glutamate transporter 1 (GLT1, j), parvalbumin (k), calbindin (l) and glutamine synthetase (GLS, m), and *in situ* hybridization against *Musashi* (d), *Notch1* (e), *Six3* (f) and *Rx* (g) in magnified fields of the boxed area in (B). GCL, the ganglion cells layer; INL, the inner nuclear layer; PR, photoreceptors and Ch, the choroid. Immunoproducts for GFP was detectable in few cells in the ectopic NR. Bar, 100 μm. The results shown are representative of more than 200 independent experiments.

expressed in the ganglion cells in the developing retina (32); Chx10, a paired-type homeobox-containing transcription factor that is expressed in bipolar cells (33); glutamate transporter 1 that removes glutamine from the synaptic cleft and is expressed in bipolar cells and terminals of PR (34); parvalbumin, a low molecular weight calcium-binding protein that is expressed in amacrine cells (35); calbindin, a calcium binding protein involved in calcium transport that is expressed in horizontal cells (35,36) and glutamine synthetase that catalyzes the amination of glutamic acid to form glutamine and is highly enriched in Muller glial cells (37). The *in situ* hybridization and immunohistochemical staining resulted in distinct staining of each type of NR neuronal and glial cells, including PR, bipolar cells, amacrine cells, horizontal cells, ganglion cells and Muller cells, at correct layers (Fig. 2C), suggesting that they were well-differentiated NR as observed in the endogenous NR. The endogenous NR attaching to the ectopic NR is slightly thinner than that attaching to the intact RPE. Fully structured NR was formed through the fundus, albeit in small spotted areas, when Pax6 was misexpressed until stage 40 (Fig. 3B). Nearly mature RPE cells lose their intracellular pigments and form a thick NR layer, in which the neuronal cell-specific genes were expressed, when Pax6(−5a) or Pax6(+5a) was misexpressed in the RPE even at stage 35–40 (Fig. 3A). The *in situ* hybridization and immunohistochemistry also showed that the ectopic NR is relatively well differentiated, which forms irregular laminar structure but contains each type of NR neuronal and glial cells (Fig. 3C).

Ectopic NR was identified histologically in 83% ($n = 393$) of the eyes transduced with *Pax6* at stage 12–24 and in 68% ($n = 196$) of eyes treated at stage 30–40. Fully structured ectopic NR was identified in 77% ($n = 250$) of morphologically altered eyes treated at stage 12–24 and in 46% ($n = 134$) of altered eyes treated at stage 30–40. Further details on the incidence of the Pax6-dependent eye architectural changes at each stage are available in Supplementary Material, Table S1. No difference was seen between two *Pax6* isoforms (either −5a or +5a) by the *in situ* hybridization and immunohistochemical analysis. Transduction of *Pax6* using an adenoviral vector or electroporation using lower dose of plasmid constructs caused similar, although somewhat weak, phenotypic changes (data not shown).